

Anders Lund · Masaru Shiotani *Editors*

Applications of EPR in Radiation Research

 Springer

Contents

Part I Elementary Radiation Processes

- 1 Fundamental Reaction Mechanisms in Radiation Chemistry and Recent Examples**..... 3
Mamoru Fujitsuka and Tetsuro Majima
- 2 Single Crystal EPR Studies of Radicals Produced by Radiolysis of Organophosphorus Compounds**..... 33
Michel Geoffroy
- 3 EPR Studies of Radical Ions Produced by Radiolysis of Fluorinated Hydrocarbons and Related Compounds in Solid Media**..... 67
Masaru Shiotani and Kenji Komaguchi
- 4 Hydrogen Molecular Ions in Solid Parahydrogen: EPR Studies at Cryogenic Temperatures**..... 117
Jun Kumagai

Part II Solid State Radiation Chemistry

- 5 EPR and IR Spectroscopy of Free Radicals and Radical Ions Produced by Radiation in Solid Systems** 151
Vladimir I. Feldman
- 6 Radiation Chemistry of Solid-State Carbohydrates Using EMR**..... 189
Henk Vrielinck, Hendrik De Cooman, Freddy Callens and Einar Sagstuen
- 7 EPR on Radiation-Induced Defects in SiO₂** 255
Antonino Alessi, Simonpietro Agnello, Gianpiero Buscarino, Yuanming Pan and Rudolf I. Mashkovtsev

Part III Biochemistry, Biophysics, and Biology Applications

- 8 Electron Spin Resonance of Radicals in Irradiated DNA** 299
Amitava Adhikary, David Becker and Michael D. Sevilla
- 9 Applications of the Spin-Trapping Method in Radiation Biology** 353
Mikinori Kuwabara, Wakako Hiraoka and Osamu Inanami

Part IV Materials Science

- 10 EPR Application to Polymers: Radiation Induced Crosslinking and Graft Polymerization** 387
Tadao Seguchi
- 11 Electronic Defects in Electron-Irradiated Silicon Carbide and III-Nitrides** 417
Nguyen Tien Son and Erik Janzén
- 12 Radiation Induced Reactions and Fragmentation in Room Temperature Ionic Liquids** 453
Ilya A. Shkrob, Timothy W. Marin and James F. Wishart

Part V Radiation Metrology

- 13 Alanine-EPR High-Dose Radiation Metrology** 489
Marc F. Desrosiers
- 14 EPR Dosimetry in Clinical Applications** 509
Eirik Malinen

Part VI Geological Applications

- 15 EPR of Primitive Organic Matter: A Tool for Astrobiology** 541
Didier Gourier, Laurent Binet and Hervé Vezin

Part VII Advanced EPR Techniques

- 16 EPR Measurement of the Spatial Distribution of Radiation Damage** 581
Michael K. Bowman, Alexander G. Maryasov and Yuri D. Tsvetkov
- 17 Study of Spin-Correlated Radical Ion Pairs in Irradiated Solutions by Optically Detected EPR and Related Techniques** 629
Vsevolod Borovkov, Dmitri Stass, Victor Bagryansky and Yuriy Molin

Part VIII Theoretical Tools

18 Uncovering Radiation Chemistry in the Solid State Through Periodic Density-Functional Calculations: Confrontation with Experimental Results and Beyond	667
Ewald Pauwels	
19 Applications of EPR and ENDOR Spectrum Simulations in Radiation Research	703
Roland Erickson and Anders Lund	
General Appendices	751
Index	763

Chapter 16

EPR Measurement of the Spatial Distribution of Radiation Damage

Michael K. Bowman, Alexander G. Maryasov and Yuri D. Tsvetkov

Abstract EPR methods to determine the nanometer-scale distribution of radiation damage products in solids are reviewed. The emphasis is on pulsed EPR methods that measure weak dipolar interactions between radiation-induced paramagnetic centers. The dipolar interactions provide a convenient ruler for distance measurement that is well-matched to the sizes of spurs and tracks created by photons and particles. The properties of dipolar interactions between paramagnetic centers are discussed with their effect on various EPR measurements. Electron spin echo measurements have determined the pair correlation function between geminate products produced by UV photolysis. Measurements on tracks of ionizing particles show that the paramagnetic centers resulting from the initial holes and electrons have quite different spatial distributions resulting from their different mobilities. Newer methods of EPR dipolar spectroscopy, particularly DEER, have considerable promise for obtaining detailed profiles of the structure of damage distributions in irradiated solids. The radius of the damage region and the number or density of paramagnetic centers created in it can be determined. Both quantities depend on LET of the radiation and can help characterize radiation for dosimetric applications and can aid in understanding the differential effects of irradiation from different sources.

16.1 Introduction

One distinctive characteristic of ionizing radiation in the condensed phase is the inhomogeneous production of initial damage products in pairs as geminate ions such as an electron and a hole. Those ions may produce additional ions as they become thermalized; the ions may recombine with their geminate partners or other radiation damage products; or they may separate and react with other molecules to form more

M. K. Bowman (✉)

Department of Chemistry, The University of Alabama, Tuscaloosa, USA
e-mail: mkbowman@as.ua.edu

A. G. Maryasov · Y. D. Tsvetkov

V. V. Voevodsky Institute of Chemical Kinetics and Combustion, Siberian Branch,
Russian Academy of Science, Novosibirsk, Russia

© Springer International Publishing 2014

A. Lund, M. Shiotani (eds.), *Applications of EPR in Radiation Research*,
DOI 10.1007/978-3-319-09216-4_16

stable products trapped in the matrix. Generally, each geminate ion is paramagnetic, having an unpaired electron spin, and unless it reacts with another paramagnetic center (PC) such as a free radical, its trapped product will also be a PC. Because the PCs are usually produced in pairs and destroyed in pairs, the spatial distribution of surviving PCs contains some information about the distribution of initial damage products as modified by transport and further reactions.

The spatial distribution of radiation-induced damage is a major factor in determining the consequences of irradiation in a number of situations: such as, mutagenesis and carcinogenesis from background radiation; radiation sterilization of pharmaceuticals and medical supplies; food irradiation; cancer radiation therapy; and even radiation dosimetry. In fact, the spatial distribution of damage is a major reason that many different types of radiation (photons, electron beams, ion beams, etc.) and energies are used for irradiation. The different initial distributions of damage products result in different biological, chemical and physical effects. The deposition of energy in condensed phases is well-characterized and can be calculated in detail. However, the transport and fate of the resulting excited states, ions and other damage products depend critically on the chemical, physical and structural properties of the material and is not readily calculable.

Electron Paramagnetic Resonance (EPR) spectroscopy has been used to study radiation-induced products with lifetimes ranging from fractions of a second to many years. EPR has most often been used in radiation chemistry to identify PC products, determine the amount of products and to measure kinetics. Yet PCs in irradiated solids have been noted as having noticeable broadening and shortened spin relaxation times attributed to dipolar interactions with the unpaired electron spins of nearby PCs. These dipolar interactions are pair-wise interactions that depend on the distance between the two interacting PCs as $1/r^3$ and are largely independent of the matter separating them. EPR methods have long been used to investigate dipolar interactions between PCs in irradiated solids and yield information ranging from 'average' dipolar field from all PCs in the sample, to dipolar spectra showing the entire range of dipolar interactions and the intensity for each. Dipolar EPR data has been interpreted in terms of average distance to the closest PC; local concentration of PCs; size and shape of spurs or tracks; and even pair distribution functions.

This chapter focuses on the measurement and characterization of dipolar interactions by EPR methods in the context of irradiated materials. We mention recent advances in pulsed dipolar spectroscopy (PDS) from the field of structural biology; techniques known variously as double electron-electron resonance (DEER), pulsed electron double resonance (PELDOR), or double quantum coherence (DQC) spectroscopies where pairs of spin labels are introduced into biomacromolecules synthetically or using site-directed spin labeling. We consider the nature and limitations of the information obtained from the various EPR methods for investigating dipolar interactions. Irradiation can produce PCs in very unusual oxidation and spin states having large anisotropy of the magnetogyric ratio (g -factor). We consider how a large g -factor anisotropy affects dipolar interactions and their measurement by EPR.

The use of EPR methods to investigate the spatial distribution of PCs in irradiated materials has a long history dating from the 1960–1970s and is well reviewed

in a number of publications [1–3]. However, experimental EPR capabilities have expanded and new approaches to the spatial distribution of radiation damage products are feasible. This chapter therefore emphasizes experimental EPR methods that appear to hold additional capabilities, tempered by consideration of possible limitations and pitfalls. We hope this prospective focus attracts researchers to ask new questions about spatial distributions and to implement and perfect the approaches outlined here.

We consider in Sect. 16.2 the dipolar interaction between PCs and how it is manifested in EPR spectra and relaxation properties, both for isotropic spins and for PCs with very anisotropic g -factors. That section may be skipped on first reading and can be supplemented by standard EPR texts. Where possible, assumptions appropriate for irradiated materials will be made. We then consider continuous-wave (CW) EPR methods for measuring dipolar interactions in Sect. 16.3; electron spin echo (ESE) based methods in Sect. 16.4; and finally recent PDS methods in Sect. 16.5. There are a number of recent sources for more information on EPR spectroscopy [4–7].

16.2 Background

The dipolar interaction is a through-space coupling between the magnetic dipoles of two PCs that is largely unaffected by the material between the PCs. The coupling perturbs the electron spin states of each PC resulting in broadening of the EPR spectrum and increased spin relaxation.

16.2.1 The Dipolar Interaction

We consider the general case of a pair of PCs with anisotropic g -tensors following Bedilo and Maryasov [8]. The spin Hamiltonian for PC₁ and PC₂ coupled by a dipole-dipole interaction is

$$\hat{H} = \hat{H}_{Z1} + \hat{H}_{Z2} + \hat{H}_{dd}^{1,2} \quad (16.1)$$

$H_{Z,i}$ describes the Zeeman interaction of PC_{*i*}'s magnetic moment with the external magnetic field B_0 directed along the laboratory Z axis [9].

$$\hat{H}_{Zi} = \beta \vec{B}_0^+ \vec{g}_i \hat{S}_i \quad (16.2)$$

The Bohr magneton is β , taken to be positive; g_i is the g -tensor of PC_{*i*}; and S_i is its vector spin operator. The cross superscript denotes the Hermitian conjugate (in this case, it reduces to transposition). Single-headed arrows indicate vectors, taken to be columns, while a double-headed arrow indicates a tensor and '^' indicates an

operator. The properties of the g “tensor” are considered in detail by Abragam and Bleaney [9]. Equation (16.2) can readily be rewritten as

$$\hat{H}_{Zi} = \beta B_0 g_{i\text{eff}} \hat{S}_{iz'} \quad (16.3)$$

where g_{eff} is the effective value of the g -tensor of the PC,

$$g_{i\text{eff}} = \sqrt{\vec{b}^+ \cdot \overset{\leftrightarrow}{g}_i \cdot \overset{\leftrightarrow}{g}_i^+ \cdot \vec{b}} \quad (16.4)$$

The unit vector along the Z axis is b and the z' axis is the direction of spin quantization by the Zeeman interaction and is parallel to

$$\overset{\leftrightarrow}{g}_i^+ \vec{b} \quad (16.5)$$

The Zeeman Hamiltonian, Eq. (16.2), is ‘solved’ (diagonalized) along the quantization axis for the PC in Eq. (16.5). Using that quantization axis, the eigenvalues $\varepsilon_{i,m}$ of the Zeeman Hamiltonian are

$$\varepsilon_{i,m} = g_{i\text{eff}} \beta B_0 m \quad (16.6)$$

where m is the projection of the PC spin onto its quantization axis, with $m = \pm 1/2$ for a PC with $S = 1/2$. The Zeeman frequency of the PC is

$$\omega_{Zi} = g_{i\text{eff}} \beta B_0 / \hbar \quad (16.7)$$

In general, the dipole-dipole interaction is between magnetic moments of two PCs with a spin Hamiltonian (see, e.g. [9])

$$\hat{H}_{dd}^{i,j} = \frac{1}{r_{ij}^3} \left[\left(\hat{\mu}_i \cdot \hat{\mu}_j \right) - 3 \left(\vec{n} \cdot \hat{\mu}_i \right) \left(\vec{n} \cdot \hat{\mu}_j \right) \right] \quad (16.8)$$

where n is the unit vector in the direction connecting the interacting PCs; r_{ij} is the intra-pair distance; and the magnetic moment operator is

$$\hat{\mu}_i = -\beta \overset{\leftrightarrow}{g}_i \hat{S}_i \quad (16.9)$$

The negative charge of electron is accounted explicitly in the above relation.

The spin Hamiltonian parameters of the coupled PCs may differ and the principal axes of the g -tensors need not coincide. In this chapter, we consider the most common case in EPR when both PCs have $S = 1/2$. Dipole coupling of high-spin PCs having significant zero-field splitting was considered in [10].

The standard approach for a weak dipole-dipole interaction [9] is to use first-order perturbation theory with a zero-order Hamiltonian consisting of the Zeeman interactions. When the two PCs have quite different EPR frequencies such cor-

rections are simple. Differences in EPR resonance frequencies may be caused by different values of g_{eff} , or by a local field from interactions with surrounding nuclei. Such local fields may be treated as a distribution of B_0 values or by a redefinition of g_{eff} . The dipolar interaction is small if

$$B_0 |g_{1\,eff} - g_{2\,eff}| \gg \frac{g_{1\,eff} g_{2\,eff} \beta}{r_{12}^3} \quad (16.10)$$

When this inequality is fulfilled, the eigenfunctions of the zero-order Hamiltonian may be written as products of the eigenfunctions of the individual PCs. To calculate the first-order correction to energy levels it is possible to replace vector spin operators in Eq. (16.9) by projections onto their quantization axes,

$$\hat{S}_i \Rightarrow \frac{\vec{g}_i^+ \cdot \vec{b}}{g_{i\,eff}} \hat{S}_{iz'} \quad (16.11)$$

and then substitute that result into Eq. (16.8) to obtain the dipolar interaction D_{12}

$$\hat{H}_{dd}^{1,2} \approx D_{12} \hat{S}_{1z'} \hat{S}_{2z'} \quad (16.12)$$

$$D_{12} = \beta^2 \frac{\left\{ \left(\vec{G}_1 \cdot \vec{b} \cdot \vec{G}_2 \cdot \vec{b} \right) - 3 \left(\vec{n} \cdot \vec{G}_1 \cdot \vec{b} \right) \left(\vec{n} \cdot \vec{G}_2 \cdot \vec{b} \right) \right\}}{r_{ij}^3 g_{1\,eff} g_{2\,eff}} \quad (16.13)$$

with the symmetric tensor G introduced by Abragam and Bleaney [9],

$$\vec{G}_i = \vec{g}_i \vec{g}_i^+ \quad (16.14)$$

The eigenvalues of the spin Hamiltonian for the pair Eq. (16.1) to first-order are functions of projections of the PC electron spins on their quantization axes,

$$\varepsilon(m_1, m_2) = \beta B_0 g_{1\,eff} m_1 + \beta B_0 g_{2\,eff} m_2 + D_{12} m_1 m_2 \quad (16.15)$$

The dipolar interaction produces a shift in each energy level proportional to D_{12} and splits each line in the EPR spectrum. Equation (16.15) is the basis for analysis of spectral changes produced in EPR spectra by weak dipolar couplings. The spectral changes appear somewhat differently in CW and pulsed EPR measurements.

16.2.2 Dipolar Features in CW EPR

The selection rules for EPR transitions caused by a weak, oscillating, CW microwave field B_1 along the laboratory X axis (perpendicular to B_0 and Z) are $\Delta m_1 + \Delta m_2 = \pm 1$ for $S = \frac{1}{2}$ PCs. This means that the spectrum of two coupled PCs consists of the sum of their individual spectra, each of which is split into a doublet with a splitting of D_{12} . A ‘weak’ mw field is weaker than D_{12} and is unable to affect both components of either doublet simultaneously. Positions of the spectral lines of the PC_i depend on the spin state of PC_j and are

$$\begin{aligned}\omega_{1z}(m_j) &= \frac{g_{i,eff}\beta B_0 + m_j D_{12}}{\hbar} \\ B_i(m_j) &= \frac{\hbar\omega_0 - m_j D_{12}}{\beta g_{i,eff}}\end{aligned}\quad (16.16)$$

for frequency-domain and for magnetic-field-domain spectra, respectively. B_i is the resonant magnetic field of PC_i , ω_0 is EPR spectrometer frequency.

If the relation in Eq. (16.10) is not fulfilled, then we have the case of ‘like’ spins with two energy levels that are nearly degenerate and may be coupled by additional pseudosecular terms of the dipole-dipole Hamiltonian containing the spin flip-flop terms, $S_{1+}S_{2-}$ and $S_{1-}S_{2+}$. This leads to larger splitting of EPR lines; in the limit of $g_{1,eff} = g_{2,eff}$ the splitting is a factor of 3/2 larger when the g -tensor anisotropy is relatively small [11] and is discussed further in Sect. 16.2.3. The behavior of ‘like’ spins is a bit more complex when g -tensor anisotropy is great ($\delta g \sim g$), but ‘like’ spins are important only in single crystals for PCs having the same orientation. In orientationally disordered systems with reasonable separations typical of irradiated materials, anisotropic PCs are always ‘unlike’.

In the high-temperature limit, when

$$\frac{\beta B_0 g_{i,eff}}{2k_B T} \ll 1 \quad (16.17)$$

the doublet of dipole-split components of PC_i have equal intensities. The high-temperature limit is valid above 4 K for nearly all EPR measurements at X- or Q-band (9.5 or 35 GHz, respectively) in irradiated materials.

It is possible to obtain the spectrum of PC_1 with isotropic g_1 -tensor split by a dipole-dipole interaction with an anisotropic PC_2 . Consider a pair with a rigid structure. The vector r_{12} connecting the two PCs has a fixed orientation and length in the principal axes of the g_2 -tensor. The transition probability of PC_1 does not depend on the pair’s orientation in the laboratory frame, so that over the narrow spectrum of PC_1 in the high-temperature limit is

$$f(B) = \sum_{m_2} \iint \delta\left(B - B_{01} + \frac{m_2 D_{12}}{\beta g_1}\right) d(\cos\theta) d\phi \quad (16.18)$$

The sum consists of just two terms corresponding to the doublet components. Here g_1 is the g -factor of the isotropic PC_1 , the angles θ and ϕ define the orientation of B_0 in the molecular frame of the anisotropic PC_2 , integration is performed over a hemisphere of possible orientations with δ the Dirac delta function, and B_{01} is the PC_1 line position in the absence of dipole coupling,

$$B_{01} = \hbar\omega_0 / \beta g_1 \quad (16.19)$$

The dipolar splitting D_{12} in Eq. (16.13) simplifies in this case where g_1 is isotropic, to

$$D_{12} = g_1 g_{2,eff} \frac{\beta^2}{r_{ij}^3} \left[1 - 3(\vec{n} \cdot \vec{b}) \frac{(\vec{n} \cdot \vec{G}_2 \vec{b})}{g_{2,eff}^2} \right] \quad (16.20)$$

The Dirac delta function in Eq. (16.18), in principle, allows integration but the result is too bulky and too complex to be useful. In practice, the requirement that g_2 and r_{12} be fixed relative to each other is rarely encountered in irradiated materials.

An even simpler equation for D_{12} occurs when the PC_2 is also isotropic with g -factor of g_2 that fulfills Eq. (16.10), so that doublets of each PC do not overlap. Equation (16.20) simplifies to the well-known relation with D_{perp} the perpendicular component of the dipolar interaction tensor

$$D_{12} = g_1 g_2 \frac{\beta^2}{r_{ij}^3} (1 - 3 \cos^2(\theta)) = D_{perp} (1 - 3 \cos^2(\theta)) \quad (16.21)$$

Omitting the normalization factor, the EPR spectrum, Eq. (16.18), for PC_1 in a pair of isotropic PCs has the shape

$$f(\Delta\tilde{B}) \propto \sum_m \int_0^1 dx \delta[\Delta\tilde{B} + m(1 - 3x^2)] \quad (16.22)$$

where $x = \cos(\theta)$, and a dimensionless lineshift is introduced,

$$\Delta\tilde{B} = r_{ij}^3 \frac{(B - B_{01})}{\beta g_2} \quad (16.23)$$

The integral in Eq. (16.22) may be calculated analytically, giving

$$f(\Delta\tilde{B}) \propto \frac{1}{\sqrt{1 + 2\Delta\tilde{B}}} \times \begin{cases} 1 & -1/2 \leq \Delta\tilde{B} \leq 1 \\ 0 & \text{otherwise} \end{cases} + \frac{1}{\sqrt{1 - 2\Delta\tilde{B}}} \times \begin{cases} 1 & -1 \leq \Delta\tilde{B} \leq 1/2 \\ 0 & \text{otherwise} \end{cases} \quad (16.24)$$

This high-temperature lineshape is known as the Pake, or Pake-like, doublet. The dipolar interaction D_{12} is a tensor with three principal values. For two isotropic PCs, the trace, or sum of the three principal values relative to the unsplit EPR line, is zero. The components have equal intensities and the average fields of both components coincide. When one or both g -tensors are anisotropic, the centers of each Pake component may differ.

Figure 16.1 shows Pake patterns for several different situations of an anisotropic PC_2 . The centers of the Pake doublet components for the isotropic PC_1 do not coincide due to the anisotropy of the g_2 -tensor. The structure of each doublet component may also vary from the standard Pake lineshape with two turning points to a lineshape with three turning points. However, it is rare to see a resolved dipolar pattern because a distribution of distances and interactions with multiple PCs will obliterate the characteristic sharp edges.

16.2.3 Dipolar Features in Pulsed EPR

Observation of Pake patterns via CW EPR are extremely rare because the Pake pattern is obscured by much larger inhomogeneous broadening. Spin echo measurements, Sect. 16.4, drastically reduce the influence of inhomogeneous broadening so that dipolar couplings can have a clear impact on the signal measured. When all the EPR transitions of a weakly-coupled pair of isotropic PCs are excited, the dipolar interaction causes a periodic modulation of the electron spin echo amplitude

$$V(\tau) \propto \cos(D_{12}\tau/\hbar) \quad (16.25)$$

Here τ is time interval between the echo-generating pulses, and D_{12} is the dipolar coupling given in Eqs. (16.13, 16.20 or 16.21). Fourier transformation of such signal produces the same Pake pattern as would CW EPR.

Analytical equations for the primary echo signal were obtained in [12] for arbitrary dipolar coupling of isotropic PCs. The equations for the echo signal are quite bulky but show that relatively weak inhomogeneous broadening decouples ‘like’ PCs. Figure 16.2 shows the frequency-domain spectrum of the oscillating echo amplitude for like PCs having a Gaussian lineshape whose dispersion σ is comparable to D_{perp} in Eq. (16.21). D_{perp} is used as the normalized frequency unit in the figure. The spectrum looks like a mixture of a standard Pake pattern with edges at D_{perp} and $2D_{perp}$ (with frequencies of 1 and 2) and a rather distorted Pake pattern with splittings $3/2$ larger at $3/2 D_{perp}$ and $3D_{perp}$. Strong coupling should be rarely encountered in irradiated materials even with rather narrow lines. The broader pattern becomes more prominent as σ decreases.

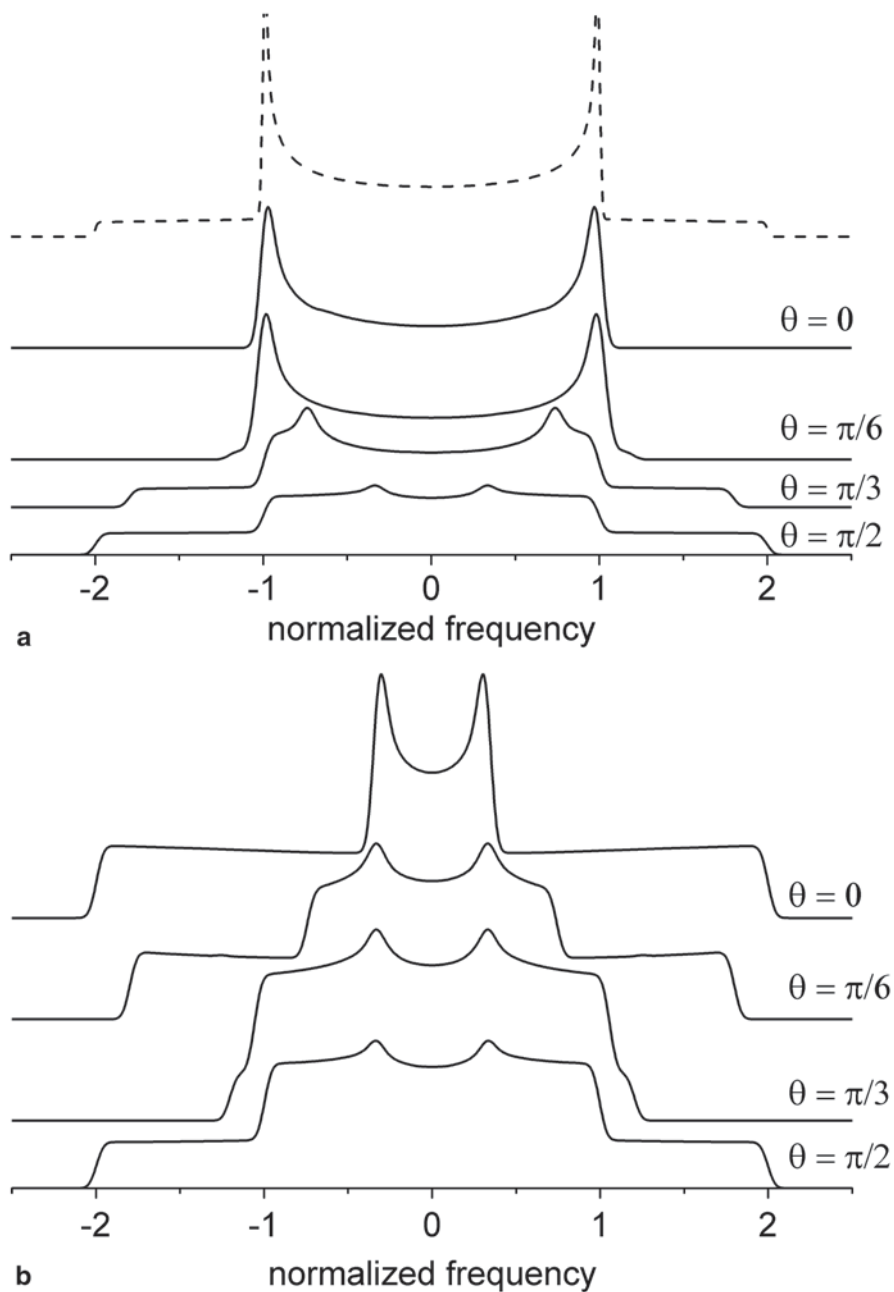
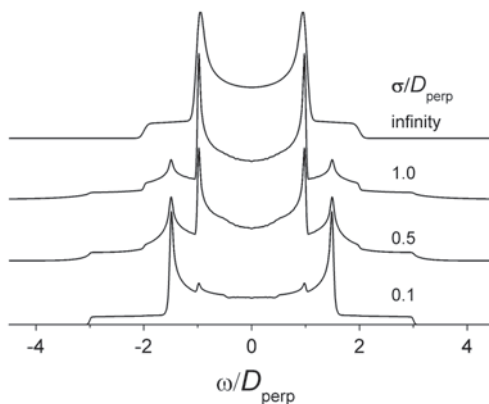


Fig. 16.1 The Pake-like patterns caused by interaction of isotropic PC with a partner having anisotropic axially symmetric g -tensor are shown in integral form. The patterns strongly depend on the pair geometry. The labels show the angle between the vector r connecting the two PCs and direction of the unique dipolar axis. **a** $g_{\text{parallel}} = 1.0$, $g_{\text{perp}} = 3.0$, standard Pake pattern is shown as dashed line for comparison; **b** $g_{\text{parallel}} = 3$, $g_{\text{perp}} = 1$

Fig. 16.2 The Pake-like pattern for a dipolar interaction D_{perp} comparable to the difference in frequencies of the $S=1/2$ PCs. The spectrum is symmetric about 0. The PCs have the same g -factors and have a Gaussian inhomogeneous broadening with a standard deviation σ . For large broadening, the pattern approaches the lineshape of Eq. 16.21



16.2.4 The Exchange Interaction

The exchange interaction J between PCs also couples spins in a similar fashion to the dipole-dipole interaction. When J is small, it can simply be added as an isotropic constant to D_{12} [13]. Fortunately, J depends very strongly on the distance between the PCs because it is proportional to the overlap between the wavefunctions containing the unpaired electrons on the two PCs. In molecular solids, J falls typically by a factor of ten for every 0.1–0.2 nm increase in separation. Beyond 1.5 nm J is considered to be negligible in comparison to the dipolar interaction [14, 15]. Strong J completely alters the EPR spectrum and will not be considered because it is unexplored territory in the measurement of distances between PCs. For isotropic PCs, the exchange interaction is isotropic and a small J appears as a non-zero trace for the measured ‘dipolar’ interaction. Yet, the trace can be non-zero for anisotropic PCs even if $J=0$ and is not a valid criterion for the presence of exchange.

16.2.5 More than one PC

When there are several PCs interacting with each other in a group, the pairwise dipolar interactions provide the PC being observed with dipolar splittings that act independently in magnetically-diluted systems. Independence of the dipolar splittings means that the spectrum of the observed PC consists of 2^{N-1} lines, when there are N PCs in the group. This means that instead of a single $\cos(D\tau)$ in Eq. (16.25) there will be a product of such cosines for the set of D_{ij} . The product can be expressed as a series of sums and differences of the D_{ij} or as a convolution of Pake doublets that quickly loses all distinctive structure. It should be noted that in EPR, broadening caused by dipole interactions in diluted systems never approaches a Gaussian lineshape as might be expected. Averaging products of cosine functions from interactions with different PCs will provide with a number of oscillating terms whose

amplitudes decay as $\ln(\tau)/\tau$, in some degenerate situations there may be also terms decaying as $\tau^{-1/2}$. These slowly decaying oscillations produce spectra with sharp or even diverging features that are definitely non-Gaussian.

16.2.6 Spatial Distributions

A number of descriptive terms such as ‘track’, ‘spur’ and ‘blob’ are used to refer to the inhomogeneous distributions of radiation damage products in solids. These terms are useful for evoking mental pictures of distributions of radiation damage, but EPR measurements of dipolar interactions are more readily discussed in terms of the radial distribution function, $f_{pc}(r)$ [3]. This is a second-order, pair-correlation function of the distances between PCs. In other fields, $f_{pc}(r)$ is known variously as the pair distribution function or pair correlation function and written as $g(r)$, $g^{(2)}(r_{12})$ or $g^{(2)}(r_1, r_2)$ which could cause some confusion with the g -factor in EPR.

The $f_{pc}(r)$ is the probability of finding one PC a distance r from another PC and can be built up by making a histogram of all inter-PC distances in a sample. If we consider having one PC at the center of a volume V , then the number $n(r)$ of PCs at a distance r is $dn(r) = f_{pc}(r)r^2 dr$. The total number, N , of PCs in the volume V (including the one at the center) and their concentration, C , are easily calculated from $f_{pc}(r)$.

$$N = \int f_{pc}(r) r^2 dr + 1$$

$$C = \frac{1 + \int f_{pc}(r) r^2 dr}{\int r^2 dr} = \frac{N}{V} \quad (16.26)$$

For a uniform or random distribution of PCs, $f_{pc}(r) = C$ for large r . On the other hand, a single radiation event, such as a single γ -ray or a single ion, can only generate a finite number of PCs, so f_{pc} must approach zero for large r . At very high doses many spatially overlapping events can approach a uniform distribution of PCs. However, f_{pc} always reaches zero at some small distance r_0 . One reason that f_{pc} must vanish is the finite size of each PC and its excluded volume—two PCs cannot occupy the same space and one is already at $r=0$. A more practical reason is that the dipolar interaction is infinite at $r=0$ and this singularity needs to be avoided in many calculations.

Near a PC it is possible to treat $dn(r)/dV(r)$ as the local concentration of PCs, representative of the typical environment of a PC, e.g., within a spur or track. EPR properties that depend on dipolar interactions are particularly well-suited for determining the local concentration because the dipolar interaction falls off very rapidly with distance, depending primarily on PCs in the immediate vicinity. We can take the uniform concentration that produces the same average dipolar broadening or spin relaxation seen in a sample and call it the local concentration [1, 16]. This definition gives a simple relation between f_{pc} and C_{loc} .

$$\begin{aligned}
 C_{loc} &= \frac{\int_{r_0}^{\infty} f_{pc}(r) D_{perp}(r)^2 r^2 dr}{\int_{r_0}^{\infty} D_{perp}(r)^2 r^2 dr} = \frac{\int_{r_0}^{\infty} f_{pc}(r) r^{-6} r^2 dr}{\int_{r_0}^{\infty} r^{-6} r^2 dr} \\
 &= 3r_0^3 \int_{r_0}^{\infty} \frac{f_{pc}(r)}{r^6} r^2 dr \quad (16.27)
 \end{aligned}$$

More than 99% total of the dipolar interaction for a uniform distribution arises from PCs in a spherical shell between r_0 and $5r_0$ from each PC.

C_{loc} is a single parameter that depends on the distance to nearby PCs and the number of nearby PCs, but determines neither quantity without additional knowledge. Yet C_{loc} is a very useful parameter. At low radiation doses, it is dominated by the characteristics of single, isolated radiation events and reflects the size and distribution of a spur, track, etc. When damage starts to overlap at high doses, C_{loc} approaches the average concentration of the sample.

C_{loc} and other related parameters, such as the second moment of the spectrum or spin relaxation rate, have long been used to estimate the dimensions of spurs and tracks in irradiated materials. When C_{loc} is plotted versus the average concentration $C_{ave} = N/V$, C_{loc} is often constant at low C_{ave} but eventually they become equal. The intersection point between these two regions is taken as the point at which the total volume of tracks, spurs, etc. equals the sample volume. With some knowledge of LET or PCs per spur, rough estimates of their dimensions can be made.

The f_{pc} has enough information to define the dimensions and number of PCs, e.g., in a spur or track. But third-order (and higher) correlations functions are needed to determine the distribution of spur sizes or the mix of spurs and tracks in a sample. It is not yet clear how to measure these higher-order correlation functions by EPR, so f_{pc} needs to be interpreted in the context of a model for the spatial distribution of PCs.

The distribution of PCs within the path of a single particle or photon is not the only factor producing the f_{pc} . Most irradiated materials contain multiple paths that are uncorrelated with each other. As the dose increases, the number of paths and their overlap increases until the dipolar contribution of PCs within a single ionization path is swamped by contributions between PCs in different paths. Yet even at low radiation doses, one can usually expect penetrating radiation to produce a background f_{pc} with a uniform distribution proportional to $r^2 dr$.

16.2.7 Scope of the Chapter

The aim of this chapter is to illustrate EPR methods that can investigate the spatial distribution of radiation-damage products in solids, the various approaches that have been used and major results that were obtained. It is intended to interest the reader in the possibilities offered by EPR rather than to be a detailed guide for making and interpreting EPR measurements. Consequently we focus on typical PC properties and measurement conditions intended to represent the vast majority of

cases. This simplifies the discussion by eliminating details restricted to rarely-encountered special cases, such as EPR measurements below 1 K.

Unless the contrary is explicitly stated, we tacitly make a number of assumptions. The PCs are assumed to have a single unpaired electron with total spin $S=1/2$ and interact with each other only by the dipolar interaction with $J=0$. The irradiated material is assumed to have no diffusion or slow motions during the measurements. The f_{pc} is taken as being isotropic and smooth, with no abrupt changes with distance so that turning points in the dipolar lineshape and characteristic dipolar modulation are smeared out and unobservable. D_{perp} is less than the difference in the unsplit EPR frequencies of the PCs involved.

Any long-range order in the material is assumed not to produce a corresponding long-range structure in f_{pc} . Higher-order correlations of PCs are taken to be insignificant. In particular, that the orientations of the g -tensors of the PCs are not correlated with each other or with the vector between the PCs, or with the magnetic field B_0 . That spin-lattice relaxation is isotropic and flip-flop transitions among the PCs are negligible. Finally, that the high-temperature limit holds so that thermal energy $k_B T$ is much greater than the energy of a microwave photon.

16.3 CW EPR Methods

The dipolar interaction between two PCs affects the CW EPR spectrum in two ways. The normal $\Delta m_s = \pm 1$ EPR transitions of each individual PC are additionally split by the dipolar interaction. The resulting spectrum is generally the convolution of the EPR spectrum of the isolated PC with a Pake-like pattern provided the orientations of the PCs are uncorrelated. New EPR absorptions also appear from transitions of the pair in which both unpaired electrons flip, the $\Delta m_s = \pm 2$ transitions which occur at approximately half the usual B_0 and are often called half-field transitions. The $\Delta m_s = \pm 2$ transitions are formally forbidden and their intensity provides an indirect measure of the dipolar interaction while their spectrum, to first order, is independent of the dipolar interaction. The intensity of the half-field transitions scales with PC separation as r^{-6} , and is generally detected only for r in the range of 0.3–1.0 nm.

When there are dipolar interactions with n other PCs, the $\Delta m_s = \pm 1$ transitions are a convolution of splittings from each of the other n PCs, giving $n+1$ (for identical dipolar splittings with the other PCs) up to 2^n transitions (for completely different dipolar splittings), but preserving the total integrated EPR intensity. The half-field transition intensity scales roughly as the sum of the intensity from each pairwise interaction.

16.3.1 Measurement of the Dipolar Spectrum

Resolved dipolar splittings from radical pairs in irradiated solids were observed by Kurita [17] and by Gordy and Morehouse [18] using radiolysis and by Lebedev [19] using UV photolysis to generate the pairs. The well-resolved dipolar splittings gave

separations of 0.3–1.0 nm between PCs. Resolved splittings from radical pairs are generally observed only under a rather restrictive set of conditions. (1) The solid has very high local order—single crystal or polycrystalline solids. The PCs are highly constrained by the structure of the solid to specific locations in the same or adjacent unit cells. (2) Irradiation and measurement is performed at low temperature, often below 77 K, to rapidly thermalize the products, and to prevent their recombination or escape. (3) Products are produced by bond cleavage or atom transfer reactions (rather than hole or electron transfer) which favor small initial separations but suppresses recombination of the thermalized products by back transfer or tunneling.

The dipolar splittings relevant to PC distributions on the multi-nanometer scale are small, less than 10 MHz and are not resolved in typical CW EPR measurements. EPR spectra are inhomogeneously broadened by *g*-factor and hyperfine anisotropy and by unresolved hyperfine interactions from hydrogen nuclei in nearby molecules so that the minimum linewidth is typically > 10 MHz. The dipolar splittings are lost in the wings of the inhomogeneous lineshape and produce no distinct features. In addition, dipolar interactions from more than one PC produce a convoluted dipolar lineshape that further smears out any distinctive structure.

Although resolved features rarely result from dipolar interactions characterizing the spatial distribution of PCs in irradiated materials, the dipolar interaction still has an impact on the EPR spectrum. There is some broadening because the resulting spectrum is a convolution of the dipolar broadening function and the EPR spectrum of an isolated, non-interacting PC. The convolution relation provides an opportunity to recover dipolar information if the EPR spectrum of isolated-non-interacting PCs can be obtained. Several different approaches have been used with some success. They generally seek to produce the same PCs at low concentration and more random distribution to minimize dipolar interactions but with the same structure, conformation and environment. One approach is to generate the same PC by another means. If the structure of heavy ion tracks is studied, production of PCs by low-dose UV-photolysis or low LET irradiation may be adequate. Irradiation at a higher temperature can increase transport before reaction or trapping and result in a more uniform distribution. The other approach starts with a non-uniform sample and mobilizes the PCs and uses diffusion to randomize the distribution and/or decrease the number of PCs through recombination or other reactions. Thermal annealing, optical bleaching/photolysis, and long-term storage have been used successfully. This second approach can be repeatedly applied to a sample until a limiting spectral shape is reached, presumably corresponding to a random distribution with minimal dipolar interactions.

The dipolar broadening spectrum can be recovered from the two EPR spectra using a Fourier deconvolution method developed for site-directed spin-labeling EPR studies. A similar problem is faced there for CW EPR spectra of biomacromolecules with one or two nitroxide spin labels attached at specific locations [20]. Rabenstein and Shin [21] divided the Fourier transforms of the EPR spectrum of the singly- and doubly-labeled biomacromolecules (with and without the dipolar interaction) to produce the Fourier transform of the dipolar broadening function. An inverse-Fourier transform then produced the dipolar broadening spectrum and this method

is used routinely in the structural biology community to analyze site-directed spin-labeling data. Occasionally the deconvolution produces a recognizable Pake-like pattern which gives the distance between labels. More often conformational flexibility results in a distribution of inter-label distances, not unlike the distribution of PC separations in irradiated solids, smoothing the features of the Pake-like pattern. Nevertheless a weighted average distance can be obtained.

The second approach is based on standard second moment theory for EPR spectra [22–24]. The second moment M_2 of a spectrum is basically its variance and has the property that the second moment of the convolution of two spectra is just the sum of their individual second moments. Subtracting the second moments of the spectra without and with dipolar interactions yields the second moment of the dipolar broadening function or $2\langle D_{perp}^2 \rangle$ for a pair with a distribution of distances.

Unfortunately, both of these procedures have a major limitation when applied to irradiated solids. The second moment or the dipolar broadening function corresponds to a distance only for a single pair of PCs. This is generally an excellent approximation for site-directed spin-labeling and some UV-photolysis experiments, but not for investigating spatial distributions of radiation-generated PCs. This limitation arises because as additional PCs interact, the total EPR spectrum is convoluted with more and more pair-wise dipolar interactions. The dipolar broadening function becomes broader and its second moment increases. Unless a Pake-like structure is resolved in the Fourier-deconvoluted dipolar broadening function, there is only a single parameter, the width or second moment, and no means to distinguish between a cluster with a few strongly-interacting PCs and a large mob of many weakly-interacting PCs. This is the same limitation that C_{loc} has and can be seen clearly for the second moment by expressing it in terms of f_{pc} or C_{loc} .

$$\begin{aligned}
 M_2 &= \int_{r_0}^{\infty} f_{pc}(r) D_{perp}(r)^2 r^2 dr = \int_{r_0}^{\infty} \frac{f_{pc}(r)}{2} \left(\frac{\mu_0}{4\pi} \frac{g^2 \beta^2}{h r^3} \right)^2 r^2 dr \\
 &= \frac{1}{2} \left(\frac{\mu_0}{4\pi} \frac{g^2 \beta^2}{h} \right)^2 \int_{r_0}^{\infty} \frac{f_{pc}(r)}{r^6} r^2 dr \\
 C_{loc} &= \frac{3}{r_0^3 D_{perp}(r_0)^2} M_2
 \end{aligned} \tag{16.28}$$

16.3.2 Non-linear Methods

There are quite a few standard and not-so-standard non-linear CW EPR methods that are sensitive to dipolar interactions. They range from progressive power saturation of the EPR signal [25, 26]; through ELDOR [27], passage effects [28] and saturation transfer [29]; to multiple quantum EPR [30]. In each approach, the intensity, and sometimes shape, of the signal depends on magnetic relaxation parameters influenced, in part, by dipolar interactions. However, these approaches are all limited by the same fundamental problem. The dipolar interaction is but one factor influencing the signal and cannot be cleanly disentangled from the other determinants

of relaxation. The evolution and relaxation of magnetization in solids is usually not accurately described by the Bloch equations that provide the starting point for quantitative analysis of non-linear CW-EPR spectroscopy. One is forced to use trends in the behavior of the EPR signal as an indication of qualitative changes in the PC f_{pc} , such as the onset of spur overlap.

16.3.3 CW EPR Results

The most extensive study of PC distribution in radiation chemistry by non-linear CW-EPR was by the Kevan group [31–41]. Power saturation of the EPR signal was used to investigate the distribution of trapped electrons, hydrogen atoms, and silver atoms, among others, in γ -irradiated frozen organic and aqueous glasses and the effect of irradiation temperature and photoexcitation. EPR saturation curves were measured for different doses and a phenomenological spin relaxation rate was extracted using simple models of the EPR response [25, 26]. The measured rate was recognized as being a complex mixture of relaxation routes, including spin-lattice relaxation, caused by interactions of a PC with the lattice, along with spin-spin interactions among the PCs. However, only spin-spin interactions should be dose dependent and only after damage from different γ -ray tracks began to overlap, providing a way to detect the onset of overlap.

The relaxation rate was constant at low radiation doses but eventually started to increase at higher doses, which was taken as the point where the spurs could completely fill the sample volume had there been no overlap. Then, assuming uniform spurs with 100 eV of energy deposited per spur, it was possible to determine the spur radius. In different aqueous and organic glasses irradiated at 77 K, the spur radius varied from 4 to > 13 nm for trapped electrons and hydrogen atoms which are fairly mobile before they are thermalized and trapped. Less mobile PCs were found to have spur radii as small as 2 nm. These studies achieved an important characterization of the size scale for spurs in these materials. Yet they rest on a very idealized spur model that misses the complex energy distribution by γ -rays.

16.4 ESE Methods

The CW EPR signal from PCs in solids depends on many parameters that are poorly understood or difficult to measure, making the study of spatial distributions inexact. Pulsed EPR has an important feature that makes measurements more convenient and more exact. Pulsed EPR provides greater control over signal generation, enabling a strategy known as refocusing. When applied properly, refocusing makes a signal independent of most interactions and allows quantitative measurement of the desired parameter, such as the distribution of dipolar fields. The principle of refocusing is demonstrated in the electron spin echo and is employed extensively in PDS.

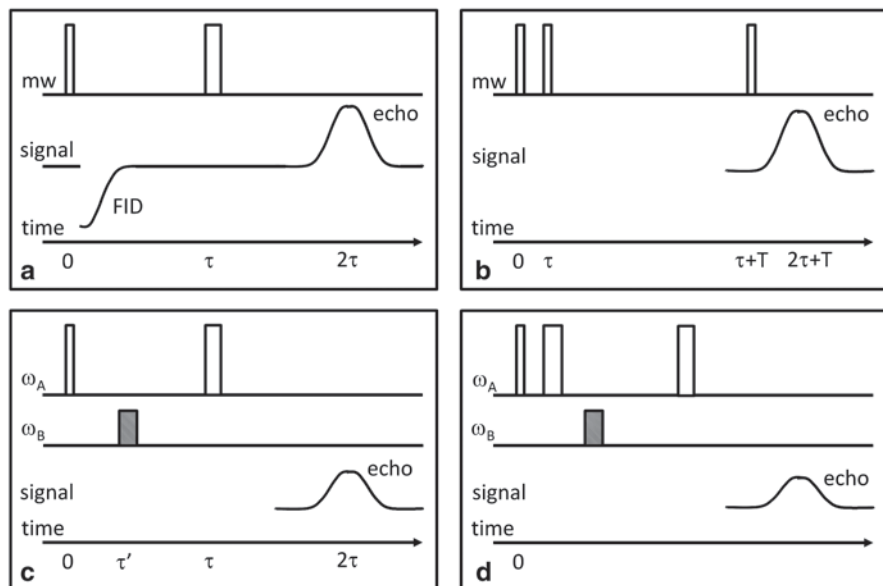


Fig. 16.3 Pulse sequences for different pulsed EPR measurements. The microwave pulse channel is labelled as mw, the signal channel shows the position of the detected echo, and a common timing convention. Typical relative widths of the microwave pulses are indicated. **a** the two-pulse or primary electron spin echo sequence with the position of the FID signal indicated, **b** three-pulse or stimulated echo, **c** three-pulse DEER experiment with the two microwave channels labelled with their frequencies, **d** four-pulse DEER sequence

Erwin Hahn produced the first spin echo [42] with nuclear spins and quickly followed with PCs. The basic experiment starts with magnetization arising from the interaction of a static, applied magnetic field and the PCs in a sample. Microwave pulses at a frequency corresponding to energy differences between spin states of the PCs are applied. The spin echo is produced by a pair of pulses separated by a short time known as τ , Fig. 16.3a. Each pulse tilts a portion of the sample magnetization, with which it is nearly in resonance, away from the applied magnetic field.

Following the first pulse, the magnetization precesses freely around the applied magnetic field, emitting a signal known as the free-induction decay or FID. The FID is a time-domain signal that is intimately related, via the Fourier Transform, to the frequency-domain CW-EPR spectrum. The FID contains much the same information about dipolar interactions and the spatial distribution as does the CW-EPR spectrum, but intertwined with all the anisotropies, inhomogeneous broadening, etc. that make quantitative dipolar studies using the CW-EPR spectrum so problematic. A sub-ensemble of PCs that have the same EPR frequency, ω , is often called a ‘spin packet’ or ‘isochromat’. Each spin packet precesses relative to the microwave frequency, ω_0 , at a rate $\Delta\omega = (\omega - \omega_0)$ so that its phase relative to the microwaves at the time of the second pulse is $\Delta\omega\tau$. The magnetization from each spin packet is rotated by the second pulse leaving it with a phase $\pi - \Delta\omega\tau$. Most things that determine the

EPR frequency of a spin packet, e.g., g -factor, hyperfine couplings, are unchanged by the microwave pulses so that $\Delta\omega$ remains unchanged. At time t after the second pulse, the spin packet has a phase $\pi - \Delta\omega\tau + \Delta\omega t$ which equals π at $t = \tau$ after the second pulse. Every spin packet has the same phase independent of $\Delta\omega$, just like all spin packets have a phase of 0 at the start of the FID. The magnetization from all the spin packets excited by the microwave pulses interfere constructively and produce a spin echo—a FID-like signal with opposite phase, τ after the second pulse and 2τ after the first.

At the center of an echo, the magnetization of each spin packet is independent of $\Delta\omega$ and the inhomogeneous broadening and anisotropies that contribute to $\Delta\omega$. The precessing magnetization is said to be refocused into an image of the FID where $\Delta\omega$ has no influence on the echo intensity at different values of τ . The echo intensity does decay at large τ , e.g., by the T_2 of the Bloch equations or the more general phase memory time T_{M^*} , but not by interactions that remain invariant during generation and formation of the spin echo. There is one notable interaction that does change—the dipolar interaction of an observed PC with other PCs in the sample, allowing the study of the spatial distribution of PCs. The dipolar interaction can change because the second microwave pulse excites the other PC, or because the other interacting PC relaxes. The change in dipolar interaction changes its contribution to $\Delta\omega$ and ω , resulting in a variation of the EPR frequency of each PC, known as spectral diffusion, and in a failure of the magnetization to completely refocus in the echo.

It is largely a matter of personal taste whether to speak of spectral diffusion as a part of T_2 or T_{M^*} decay of the spin echo or as a separate process, but for convenience, we will consider them as separate. The primary reason for doing so is to split the decay of the spin echo $V(\tau)$ into the product of two terms: the ‘intrinsic’ relaxation of the PC in isolation, V_{int} ; and the decay resulting from spectral diffusion and dipolar interactions, V_{SD} . Usually, the intensity of the spin echo appearing at the time 2τ can be expressed as a product.

$$V(\tau) = V_{\text{int}}(T_{M^*}, \tau) V_{\text{SD}}(\tau) \quad (16.29)$$

It is much easier to separate these two quantities in experimental spin echo decays than it is to extract quantitative dipolar information from CW EPR spectra or saturation studies. The spin echo experiment refocuses most interactions that have no bearing on dipolar interactions, makes the echo signal decay independent of those extraneous interactions, and allows a clean determination of the pertinent dipolar interactions.

This two-pulse, or primary, echo experiment has been expanded into a large family of experiments to measure different PC properties, with more pulses and/or microwave frequencies, and refocusing as many extraneous influences as possible. Some of these experiments are discussed later in this chapter. When discussing pulsed measurements, it is common to distinguish the PCs that produce the measured EPR signal (known as A spins) from the PCs that have dipolar couplings to and affect the A spins (B spins). This is not always a unique distinction because

some PCs act as both A and B spins while others are neither A spins nor affect the A spins.

16.4.1 Spectral Diffusion

Spectral diffusion is a general term for the variation of the EPR frequency of a PC with time. It can arise from a variety of causes unrelated to the spatial distribution of PCs, e.g., molecular motion of the PC or the surrounding matrix, or nuclear spin diffusion of matrix nuclei which are typically considered parts of the intrinsic V_{int} relaxation of the PC. Although spectral diffusion enters into many pulsed experiments, it is most often studied using the primary echo.

Nuclear spin diffusion makes an important contribution in nearly all samples because PCs have weak, but non-zero hyperfine interactions (primarily dipolar) with nuclear spins even a few nanometers away [1, 43]. Flip-flops (T_2 -like events) between nuclear spins modulate the net hyperfine interaction and EPR frequency of the PC. Although the hyperfine interaction with any distant nuclear spin is weak and the rate of flip-flops is slow, there are large numbers of nuclei that potentially participate. Decay of the spin echo is often dominated by nuclear spin diffusion for PCs in samples with significant aqueous or organic components. Depending on its rate and the strength of the hyperfine interaction with the PC, the spin echo decay from nuclear spin diffusion often has the form $\text{Exp}[-(2\tau/T_M)^n]$ where n lies between 1.75 and 3 [2]. Deuteration of the sample, replacing ^1H with ^2H , slows V_{int} relaxation in most cases by decreasing $1/T_M$ and n , but may perturb the spatial distribution, e.g., by affecting thermalization of holes and electrons or the rate of hydrogen abstraction.

Spectral diffusion arising from dipolar interactions between PCs is more relevant to the study of spatial distributions. Spectral diffusion can occur if the second microwave pulse generating the spin echo also affects B spins with a dipolar coupling to the A spins. This can happen when the B spin's EPR frequency is close to that of the microwave pulse. In that case, the spectral diffusion occurs at the instant of the second microwave pulse and is known as 'instantaneous' diffusion. Spectral diffusion can also take place as a result of flip-flops between B spins or from the spin-lattice (T_1) relaxation of nearby B spins which can occur one or more times during the entire 2τ of the echo-generating sequence.

16.4.1.1 Instantaneous Diffusion

Instantaneous diffusion was treated by Klauder and Anderson [44] for a homogeneous distribution of PCs and was later generalized for a uniform distribution in a lower dimensional object such as a plane or a line by Milov et al. [13]. Instantaneous diffusion can be expanded from the response of an A spin with a dipolar coupling to a B spin [45–47]. The contribution to the primary echo response is

$$\begin{aligned}
V_{pair,B}(\tau) &= Tr\left(\hat{\rho}_{A,B} \hat{S}_{Ay}\right) \\
&= \left[\cosh(R_B \tau) + \frac{W_B}{R_B} \sinh(R_B \tau)\right]^2 \\
&\quad + \frac{D_B^2}{4R_B^2} \sinh(R_B \tau)^2 (1 - 2p_B) e^{-2W_B \tau}
\end{aligned} \tag{16.30}$$

The density matrix for the pair composed of the A and B spin is $\rho_{A,B}$, the dipolar coupling between the pair of PCs is D_B , W_B is the rate at which S_z of the B spin changes, $R_B^2 = W_B^2 - D_B^2/4$ and p_B is the probability that the second microwave pulse flips the B spin. The instantaneous diffusion is distinguished from all other types of relaxation of the spin echo by its dependence on p_B . If the B spin relaxes very rapidly so that $W_B \tau \gg 1$, then $V_{pair,B}(\tau)$ becomes independent of p_B and that A spin no longer contributes to instantaneous diffusion. On the other hand, if $W_B \tau \ll 1$ for the measured range of τ , it is possible to set $W_B = 0$ and obtain the instantaneous diffusion signal

$$\begin{aligned}
V_{ID}(\tau) &= V_{pair,B}(\tau) = 1 - 2p_B \sin\left(\frac{D_B \tau}{2}\right)^2 \\
&= 1 - p_B (1 - \cos(D_B \tau))
\end{aligned} \tag{16.31}$$

If an intermediate value of W_B results from flip-flops transitions and interactions with other B spins, then higher-order correlation functions and not just the simple radial distribution function are involved; this case will not be considered here. However, if W_B is determined by spin-lattice relaxation of the isolated B spin, it can be slowed by decreasing the measurement temperature until $W_B \tau \ll 1$, to allow use of Eq. (16.31) rather than (16.30).

Each A spin typically interacts with more than one B spin. The instantaneous diffusion decay of the A spin from its interactions with all the B spins in the sample (or more generally the spectral diffusion decay when $W_B > 0$) is

$$V_{SD}(\tau) = Tr\left(\hat{\rho} \hat{S}_{Ay}\right) \tag{16.32}$$

A major simplification is possible as long as interactions among the B spins can be ignored, i.e., neglect of all dipolar and exchange interactions that do not involve the A spin. Such a situation can occur in magnetically dilute solids. The density matrix of the system is just the tensor product of density matrices for the pairwise interaction of the A spin with each of the B spins in the sample. And V_{SD} or V_{ID} is simply the product of the individual V_{pair,B_i} terms [48].

$$\begin{aligned}
\hat{\rho} &= \hat{\rho}_{A,B_1} \times \hat{\rho}_{A,B_2} \times \cdots \times \hat{\rho}_{A,B_i} \times \cdots \\
Tr\left(\hat{\rho} \hat{S}_{Ay}\right) &= \prod_i Tr\left(\hat{\rho}_{A,B_i} \hat{S}_{Ay}\right) \\
V_{SD}(\tau) &= \prod_i V_{pair,B_i}(\tau)
\end{aligned} \tag{16.33}$$

This is an important result that allows expression of spectral diffusion as a product of terms, for example, from PCs within the same spur or track and from PCs of different tracks, or for different radiation damage products. However, this result is possible only if all pairwise interactions that do not involve the A spin can be ignored. In particular, it does not allow dipolar and exchange interactions responsible for spin diffusion, spin flip-flops and cross relaxation among the B spins. When their rate, W_B , is not negligible, as in samples known as ‘ T_2 ’-type, Eq. (16.33) does not apply. Therefore we focus on ‘ T_1 ’-type samples at temperatures where W_B is negligible. Instantaneous diffusion can also be observed through the stimulated echo. The theory has been developed [1, 2, 43, 44] but will not be discussed here because it is rarely used to determine spatial distributions.

16.4.1.2 Uniform Distribution

Equation (16.33) enables calculation of $V_{ID}(\tau)$ for $W_B=0$, from a uniform distribution of PCs by averaging Eq. (16.31) over all possible distributions of B spins. If the second term in Eq. (16.31) is small, which can always be achieved at $p_B \ll 1$,

$$\begin{aligned} V_{pair,B}(\tau) &= 1 - p_B (1 - \cos(D_B \tau)) \\ &\approx e^{-p_B(1 - \cos(D_B \tau))} \\ V_{ID}(\tau) &= V_{SD}(\tau, (W_B = 0)) \\ &= \prod_i V_{pair,B_i}(\tau) \approx \prod_i e^{-p_{B_i}(1 - \cos(D_{B_i} \tau))} \\ &= e^{-\sum_i p_{B_i}(1 - \cos(D_{B_i} \tau))} \end{aligned} \quad (16.34)$$

If the probability, p_B , of flipping the spin of a B spin by the second microwave pulse is the same for all B spins, then for a uniform distribution of PCs, the spin echo decay due to instantaneous diffusion is

$$\begin{aligned} \langle V_{ID}(\tau) \rangle &= \left\langle e^{-\sum_i p_{B_i}(1 - \cos(D_{B_i} \tau))} \right\rangle = e^{-p_B \sum_i \langle 1 - \cos(D_{B_i} \tau) \rangle} \\ &= e^{-p_B \int_0^\infty \int_0^{\pi/2} (1 - \cos(D_B(r, \theta) \tau)) r^2 \sin(\theta) d\theta dr} \\ &= e^{-2\tau p_B \left(\frac{4\pi^2 g^2 \beta^2}{9\sqrt{3} h} C \right)} = e^{-2\tau p_B k_{ID}} = e^{-2\tau p_B \alpha C} \end{aligned} \quad (16.35)$$

C is the concentration of B spins having this uniform distribution and the angular brackets indicate an average over the appropriate distribution. For A and B spins having a g -factor of about 2.0 and $S = 1/2$, α in Eq. (16.35) approaches $8.2 \times 10^{-13} \text{ cm}^3 \text{ s}^{-1}$. This exponential decay is proportional to the Fourier Transform of the nearly Lorentzian dipolar spectrum [9]. We note that the second moment of this Lorentzian spectrum is infinite if the excluded volume is ignored when integrating

over r in Eq. (16.35). This is a feature common to magnetically-diluted systems; estimates of the second moment do not converge smoothly. The rate of decay in Eq. (16.35) is proportional to the dipolar interaction between spins at the distance given by $\langle 1/r^3 \rangle = C$.

Other sources of echo decay, such as instantaneous diffusion from other B spins, spectral diffusion, spin relaxation and even ESEEM, contribute multiplicatively to the decay of the echo during the time period 2τ . However, only instantaneous diffusion depends on p_B and this dependence is used to extract the instantaneous diffusion from all other sources of echo decay. The p_B can be calculated if the EPR spectrum, $g(\omega_0)$, of the B spins is known and the microwave field, ω_1 , is uniform.

$$p_B = \left\langle \sin\left(\frac{\omega_1 t_p}{2}\right)^2 \right\rangle = \int_0^\infty \frac{\omega_1^2 I(\omega_0)}{\omega_1^2 + (\omega - \omega_0)^2} \sin\left(\frac{t_p}{2} \sqrt{\omega_1^2 + (\omega - \omega_0)^2}\right)^2 d\omega_0 \quad (16.36)$$

It is best if small samples are used so that ω_1 is uniform over the sample. A distribution of ω_1 affects both excitation of the signal and the efficiency of detection of the echo signal from that region of the sample. In addition, A spins with different ω_1 decay at different rates in Eq. (16.35) so that the overall decay can be non-exponential.

Equation (16.35) yields a simple result from a simple integration, but includes the very unrealistic assumption that a uniform distribution of B spins extends beyond the sample to infinite distances. For macroscopic samples, the extension of the averaging to infinity is justifiable. Distant B spins have tiny dipolar interactions so that $D_i\tau$ is insignificant during the $\tau = 0.1\text{--}10 \mu\text{s}$ range of typical spin echo measurements and the very distant B spins have no effect on echo decay. Therefore, sample size and shape are irrelevant for instantaneous diffusion with uniform distributions. At the other integration limit, very close B spins have an immediate effect on the spin echo of the A spin. A pair of PCs with random orientation, θ , relative to the applied magnetic field produces an average decay [49] expressed in terms of C and S , the Fresnel sine and cosine integrals respectively [50]

$$\begin{aligned} \langle V_{pair,B}(\tau) \rangle_\theta &= 1 - p_B \langle 1 - \cos(D_B \tau) \rangle_\theta \\ &= 1 - p_B \left(1 - \frac{\cos\left(\frac{\pi y}{6}\right) C(\sqrt{y}) + \sin\left(\frac{\pi y}{6}\right) S(\sqrt{y})}{\sqrt{y}} \right) \\ y &= \frac{6D_{perp}\tau}{\pi} \end{aligned} \quad (16.37)$$

The factor following p_B approaches unity at large τ and exceeds 0.8 after about $0.15 \mu\text{s}$ for a pair of PCs with $g \sim 2.0$ separated by 3 nm. That suggests the exponential

decay limit in Eq. (16.35) requires $p_B < 0.1$. Fortunately the major deviation is at even shorter times, within the deadtime of the measurement. Provided that the distribution of B spins is not highly correlated, the principal consequence of exciting an extremely close B spin with the second microwave pulse is to cause the A spin to disappear; leaving the measured echo to decay according to Eq. (16.35) during the experimentally accessible time window.

The distribution of B spins cannot be uniform at short distances for a number of reasons mentioned in Sect. 16.2.4. Any distribution must go to zero for distances smaller than some r_0 but affects the spin echo decay only at short times that typically are lost in the deadtime of a spin echo measurement. Klauder and Anderson [44] calculated that the echo decay from instantaneous diffusion by a uniform distribution of B spins with an r_0 is initially Gaussian but smoothly becomes the exponential decay in Eq. (16.35), which explained earlier experimental observations by Mims et al. [51].

16.4.1.3 Within the Track or Spur

The contribution of uniformly-distributed PCs to instantaneous diffusion is multiplied by a similar decay for PCs within the same track or spur. It then becomes necessary to average $V_{ID}(\tau)$ over the $f_{pc}(r)$ for the track or spur in the limit of $p_B < 0.1$ as

$$\begin{aligned} \langle V_{ID}(\tau) \rangle &= e^{-p_B \int_0^\infty f_{pc}(r) \int_0^{\pi/2} (1 - \cos(D_B(r, \theta)\tau)) r^2 \sin(\theta) d\theta dr} \\ &= e^{-p_B \int_0^\infty f_{pc}(r) \langle 1 - \cos(D_B(r, \theta)\tau) \rangle_\theta r^2 dr} \end{aligned} \quad (16.38)$$

This contains the same average in angular brackets encountered in Eq. (16.37). If the functional form of f_{pc} is known, Eq. (16.38) can be evaluated and parameters of the distribution determined, but if f_{pc} is not known, there seems to be limited information available. For small values of τ , the cosine function can be expanded, while for long τ , the term in brackets approaches unity, giving two asymptotic limits. The decay is initially Gaussian, yielding the average dipolar interaction, and at long times becomes constant, giving the number ($N+1$) of PCs ‘in’ the spur or track. For PCs with $g \sim 2.0$, D in MHz and r in nm, the limiting forms are

$$\langle V_{ID}(\tau) \rangle \approx \begin{cases} e^{-p_B 13.3 \tau^2 \int_0^\infty f_{pc}(r) D_{perp}^2 r^2 dr} \rightarrow e^{-p_B 13.3 N \langle D_{perp}^2 \rangle \tau^2}, & \tau \rightarrow 0 \\ e^{-p_B \int_0^\infty f_{pc}(r) r^2 dr} \rightarrow e^{-p_B N}, & \tau \rightarrow \infty \end{cases} \quad (16.39)$$

Salikhov et al. [52] place the break between the short- and long-time behavior at the time $t^* = 2.5/D_{perp}$. To observe part of the early, Gaussian decay of Eq. (16.39) in the spin echo with a spectrometer deadtime of 0.1 μ s requires $D_{perp} < 4$ MHz ($r > 2.5$ nm for $g \sim 2.0$ PCs). To reach the constant, long-time limit by $\tau = 10$ μ s requires $D_{perp} \gg 0.04$ MHz ($r < 10$ nm). Instantaneous diffusion actually probes a narrow distance range of roughly 2.5–10 nm which is similar to the diameter of spurs and tracks.

16.4.1.4 Other Spectral Diffusion

Instantaneous diffusion represents the limit in which dipolar interactions change only as a result of the second microwave pulse. The opposite limit occurs when p_B approaches zero and spectral diffusion occurs by spin relaxation of the B spins.

‘ T_1 ’ Samples

The S_z component of a B spin is part of the dipolar interaction and can change through spin-lattice relaxation. The rate W_B is assumed to be the same for all B spins of the same type. The echo response for an A spin coupled to a relaxing B spin can be calculated using Eq. (16.30) with $p_B=0$. The response reaches limiting cases for W_B much smaller or much larger than the dipolar interaction. The echo decays at W_B for large dipolar interactions while there is ‘motional averaging’ or decoupling of the dipolar interaction for $W_B \gg D_B$.

$$V_{pair,B}(\tau) = \left[\cosh(R_B \tau) + \frac{W_B}{R_B} \sinh(R_B \tau) \right]^2 + \frac{D_B^2}{4R_B^2} \sinh(R_B \tau)^2 \Big] e^{-2W_B \tau}$$

$$= \begin{cases} e^{-2W_B \tau}, & W_B \ll D_B \\ e^{-2\frac{D_B^2}{8W_B} \tau}, & W_B \gg D_B \end{cases} \quad (16.40)$$

The echo decay for a sample can be derived as in Eqs. (16.34 and 16.35) for a uniform distribution to give

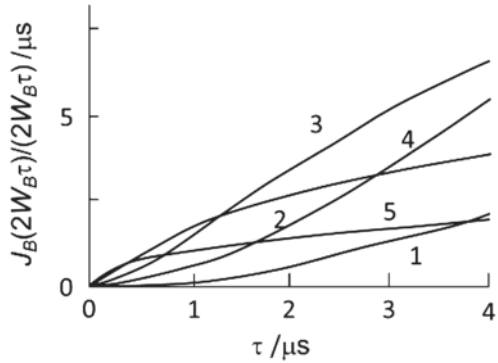
$$\langle V_{SD}(\tau) \rangle = e^{-\frac{9\sqrt{3}}{4\pi^2} \alpha C \frac{J_B(2W_B \tau)}{2W_B}} \quad (16.41)$$

The J_B function has been derived and experimentally verified a number of times [1, 43, 45, 53–55]. For τ in the range of 0.4–4.0 μ s, $J_B(2W_B \tau)/(2W_B)$ is largely linear, giving a nearly exponential decay for $\langle V_{SD} \rangle$ although the slope does vary, Fig. 16.4. The asymptotic forms are known along with the limiting decay functions.

$$J_B(2W_B \tau) = \begin{cases} \frac{16\pi^2}{9\sqrt{3}} W_B^2 \tau^2, & W_B \tau \ll 1 \\ \frac{16\pi^2}{9\sqrt{3}} W_B \sqrt{\frac{\tau}{\pi W_B}}, & W_B \tau \gg 1 \end{cases}$$

$$\langle V_{SD}(\tau) \rangle = \begin{cases} e^{-2\alpha C W_B \tau^2}, & W_B \tau \ll 1 \\ e^{-2\alpha C \sqrt{\frac{\tau}{\pi W_B}}}, & W_B \tau \gg 1 \end{cases} \quad (16.42)$$

Fig. 16.4 Plot of $J_B(2W_B\tau)/(2W_B)$ versus τ for various values of W_B : 1) $0.3 \times 10^5 \text{ s}^{-1}$, 2) $1.25 \times 10^5 \text{ s}^{-1}$, 3) $5.0 \times 10^5 \text{ s}^{-1}$, 4) $2.0 \times 10^6 \text{ s}^{-1}$, 5) $8.0 \times 10^6 \text{ s}^{-1}$



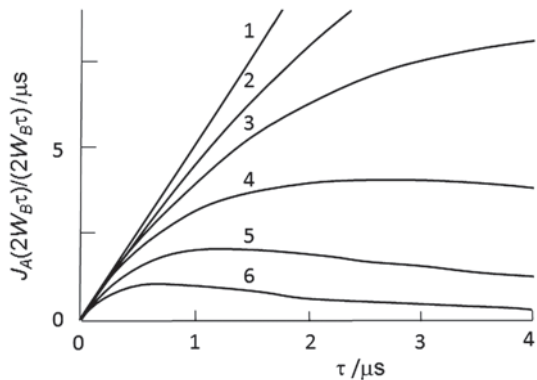
Determining a non-uniform distribution is a challenge. The two limits in Eq. (16.40) show that distant B spins do not contribute to the echo decay while all close B spins make precisely the same contribution. Fortunately, the transition between these two regions occurs rather abruptly. Calculations by Raitsimring and Salikhov [3] suggest that the transition occurs over a change in distance of only a factor of two. They suggest that the echo intensity at large $W_B\tau$ measures the fraction of A spins which lacks a nearby B spin with $D_B > W_B$. This effect enables estimation of f_{pc} for PCs in pairs or small clusters by systematic variation of $W_B\tau$.

The echo decay caused by spectral diffusion was calculated for a uniform distribution with finite p_B [3, 45]. An additional term appears in Eq. (16.41) (Fig. 16.5).

$$\langle V_{SD}(\tau) \rangle = e^{-\frac{9\sqrt{3}}{4\pi^2} \alpha C \frac{J_B(2W_B\tau) + p_B J_A(2W_B\tau)}{2W_B}}$$

$$J_A(2W_B\tau) = \begin{cases} \frac{16\tau^2}{9\sqrt{3}} W_B\tau, & W_B\tau \ll 1 \\ 0, & W_B\tau \gg 1 \end{cases} \tag{16.43}$$

Fig. 16.5 Plot of $J_A(2W_B\tau)/(2W_B)$ versus τ for various values of W_B : 1) 0 s^{-1} , 2) $0.625 \times 10^5 \text{ s}^{-1}$, 3) $1.25 \times 10^5 \text{ s}^{-1}$, 4) $2.5 \times 10^5 \text{ s}^{-1}$, 5) $5.0 \times 10^5 \text{ s}^{-1}$, 6) $1.0 \times 10^6 \text{ s}^{-1}$



For irradiated samples with more than one type of B spin, there are different $\langle V_{SD} \rangle$ for each type which are all multiplied together, each with its appropriate values of C , W and p .

‘ T_2 ’ Samples

Spin relaxation is considerably more complicated in solid samples of dilute PCs than in the simple Bloch equation model [56]. S_z can change by a mutual flip-flop with another nearby PC having the opposite value of S_z . This is often called spin diffusion since it involves the migration of a spin but not the PC, however in the context of spectral diffusion measurements, it is often referred to as a T_2 event. The flip-flops are made possible by dipolar and exchange interactions so their rate is strongly dependent on the distance between the two PCs involved. Typically there will be a broad distribution of flip-flop rates in a sample, because each PC does not have the same distribution of PCs around it. In these ‘ T_2 ’ samples the decay of the A spins depends on the distribution of B spins around it AND the distribution of PCs around the B spins, in other words, third-order correlation functions. Because each flip-flop involves two B spins, their dipolar interactions with the observed A spin are not uncorrelated which further complicates the calculation of $\langle V_{SD} \rangle$.

Calculations have been made for these ‘ T_2 ’ samples for a uniform distribution of B spins, resulting in an equation for $\langle V_{SD} \rangle$ analogous to Eq. (16.43) with J_A and J_B replaced by Q_A and Q_B [3, 45]. The derivations of Q_A and Q_B use a phenomenological distribution for W_B that is uncorrelated with D values and the distribution of PCs, and also does not account for correlations between terms appearing in both Q_A and Q_B .

16.4.1.5 Spectral Diffusion Kernel

The stimulated echo is produced by three microwave pulses with a separation of τ between the first pair and T between the second and third pulses, Fig. 16.3b. The stimulated echo appears τ following the final pulse and its normalized intensity is represented as $V(\tau, T)$. Mims [43, 57] noted that for ‘ T_1 ’ samples for $W_B \tau$ and $W_B T \ll 1$, the Fourier transform of $V(\tau, T)/V(\tau)$ is the spectral diffusion kernel, $K_{SD}(\Delta\omega, T)$.

The spectral diffusion kernel indicates how much the EPR frequency of a PC has changed in the time T [58]. A slice from K_{SD} taken at $T \ll 1/W_B$ gives the spectrum of dipolar interactions which could be deconvoluted to give f_{pc} . Such an approach would be expected to work best for relatively small clusters of PCs. This experimental approach was used by Kulik et al. [59] as the basis for the RIDME method which has been applied to PC pairs in biological systems [60–68].

16.4.2 Cross Relaxation

Dipolar interactions between PCs can produce a change in S_z in one or both PCs. When this results in flip-flops among PCs of the same type it is called spin diffusion. But if it is between distinctly different PCs, particularly if one has a fast spin-lattice relaxation rate, it is often called cross relaxation. Both phenomena can be extremely complex, depending on the EPR spectra of both PCs, T_1 , T_2 and the interaction D_B .

A common situation is where B spins are a different type of PC with rapid T_1 and act as a relaxation sink. The A spins are excited or inverted by a microwave pulse and their relaxation is monitored in time. There are two important limiting cases. One occurs when spin diffusion among the A spins is much faster than cross relaxation to the B spin relaxation sink. The A spin relaxation is exponential. On the other hand, when spin diffusion is negligible, the rate of cross relaxation for each A spin is proportional to its strongest D_B^2 . If the f_{pc} between A and B spins is uniform, relaxation of the A spins has the well-known kinetics for any dipolar-mediated quenching: $\exp[-(k t)^{1/2}]$. If the sample is composed of dilute pairs of PCs, there is some possibility of extracting f_{pc} [69, 70] although uncertainty as to the angular dependence of cross relaxation can complicate matters [71].

16.4.3 Experimental Studies

An early focus of the electron spin echo spectrometer at the Institute of Chemical Kinetics and Combustion in Novosibirsk, Russia was the study of relaxation and spatial distribution of PCs in irradiated frozen solids. That effort helped develop and validate many of the spin echo methods described here in Sect. 16.4. The experimental work has been reviewed a number of times [1–3]. It is amazing what was accomplished without the sensitivity of modern instruments, without modern computer applications and with analog data taken by hand from chart paper. Considerable information was derived by varying radiation dose and the type of radiation from UV, which could produce only one PC pair per photon, to ^{60}Co γ -rays, which produce a trail of spurs, as well as neutrons and β -, α - and fission particles spanning almost three orders of magnitude in LET.

16.4.3.1 Validation

Detailed investigations of spin-lattice relaxation of hydrogen atoms trapped in amorphous quartz at 77 K have been made [72, 73]. At sufficiently low hydrogen atom concentrations, the main echo decay is due to T_1 . The spin-lattice relaxation kinetics of the hydrogen atoms is $\exp(-a t^{1/2})$. There is a distribution of spin-lattice relaxation times caused by cross relaxation to a fast relaxing PC in the quartz. The most probable value of T_1 for hydrogen atoms is 2×10^{-2} s at 77 K and about 100 s at

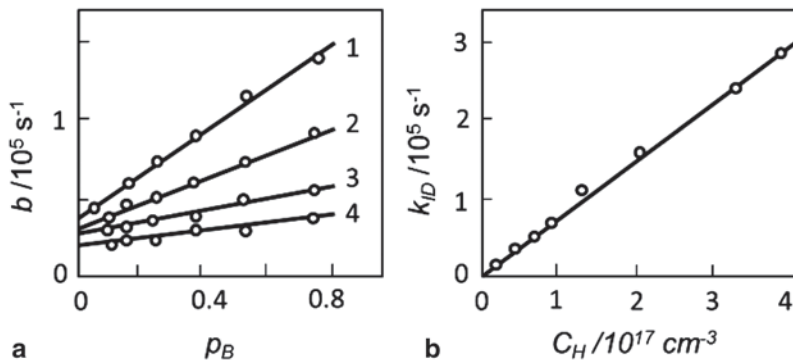


Fig. 16.6 **a** The p_B dependence of the echo decay rate b of hydrogen atoms for various concentrations of hydrogen atoms in γ -irradiated fused quartz at 77 K: (1) $3.8 \times 10^{17} \text{ cm}^{-3}$, (2) $2.0 \times 10^{17} \text{ cm}^{-3}$, (3) $0.9 \times 10^{17} \text{ cm}^{-3}$, (4) $0.5 \times 10^{17} \text{ cm}^{-3}$, **b** Instantaneous diffusion rate k_{ID} versus the hydrogen atom concentration. The slope is α

4.2 K. Because of weak interaction between hydrogen atoms and the lattice, instantaneous diffusion should be the main mechanism of two pulse ESE signal decay.

The two-pulse echo decay of hydrogen atoms trapped in glassy quartz at 77 K was studied at various hydrogen atom concentrations and p_B . The EPR spectrum consists of two lines separated by the hyperfine coupling of 50.5 mT, each line having a linewidth at 77 K of 0.03 mT. Either hydrogen line could be uniformly excited. The spin echo decay kinetics for hydrogen atoms are described by the simple exponential function

$$\begin{aligned} V(\tau) &= e^{-2\tau b(C_H)} = e^{-2\tau \left(b_0 + \frac{p_B}{2} k_{ID} \right)} \\ &= e^{-2\tau b_0} e^{-2\tau \frac{p_B}{2} \alpha C_H} \end{aligned} \quad (16.44)$$

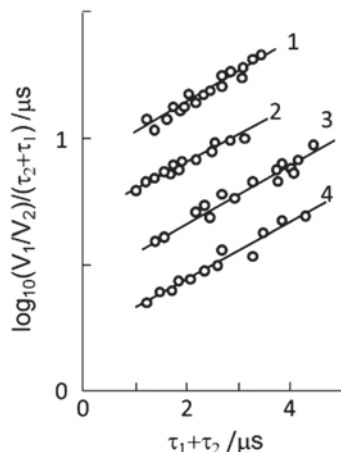
C_H is the hydrogen atom concentration in the sample and α was found to be $8 \times 10^{-13} \text{ C}_H \text{ cm}^3 \text{ s}^{-1}$, where p_B is calculated for one and not both of the hydrogen atom lines, introducing the factor of 1/2. The decay rates are plotted in Fig. 16.6 and show that the echo decay is caused by instantaneous diffusion from a uniform distribution of hydrogen atoms.

Two types of PCs, H atoms and SO_4^- ion radicals, are stabilized at 77 K in irradiated solutions of 8 M sulfuric acid. The two-pulse spin echo decay of the hydrogen atoms [74] is

$$V(\tau) = e^{-2\tau b - m\tau^2} \quad (16.45)$$

The experimental data falls on a straight line when it is plotted in special coordinates, providing good evidence for the validity of Eq. (16.45). The values of m were determined from the slopes of the straight lines, and the values for b were obtained from the intercepts (Fig. 16.7).

Fig. 16.7 Kinetics (linear plot) of hydrogen atom spin echo decay in irradiated sulfuric acid at 77 K for various hydrogen atom concentrations (cm^{-3}): (1) $2.4 \times 10^{18} \text{ cm}^{-3}$, (2) $2 \times 10^{17} \text{ cm}^{-3}$, (3) $2.2 \times 10^{17} \text{ cm}^{-3}$, (4) $2 \times 10^{17} \text{ cm}^{-3}$. V_1 and V_2 are the amplitudes of the ESE signal corresponding to the times τ_1 and τ_2



The $\exp(-m \tau^2)$ term in the decay is indicative that nuclear spin diffusion among the matrix protons contributes significantly. The parameter m is independent of the PC concentrations and equals $2.6 \times 10^{11} \text{ s}^{-2}$. This is in good agreement with the theoretical values and m depends on the matrix proton concentration as $m = 7 \times 10^{-35} \text{ cm}^6 \text{ s}^{-2} C_{\text{proton}}^2$ in the 8 M H_2SO_4 .

The SO_4^- ion radicals in the frozen γ -irradiated sulfuric acid solutions were investigated [45] over a wide range of concentrations and temperature. The main contribution to their echo decay at low concentrations ($\sim 10^{17} \text{ cm}^{-3}$) is from nuclear spin diffusion and from their own spin-lattice relaxation. This system can be regarded a ' T_1 '-sample. At high concentrations of $\text{SO}_4^- (> 5 \times 10^{18} \text{ cm}^{-3})$ an additional decay component appeared, corresponding quantitatively to the spectral diffusion of Eq. (16.43).

These studies were conducted at high doses where the overlap of spurs and hydrogen atom diffusion before trapping was expected to produce a uniform distribution. In fact, the shapes of the decays are those expected for a uniform distribution. The echo decay could be measured over the limited range of $\tau \sim 0.3\text{--}5 \mu\text{s}$. At shorter τ , the echo was obscured by the ringing of the cavity and switching transients and at longer τ , the echo had decayed into the noise. The expected drop in f_{pc} at short distances would be apparent only during the $0.3 \mu\text{s}$ deadtime. These measurements confirmed the theory for echo decay caused by instantaneous diffusion and by spectral diffusion in ' T_1 ' and to a lesser extent ' T_2 ' samples.

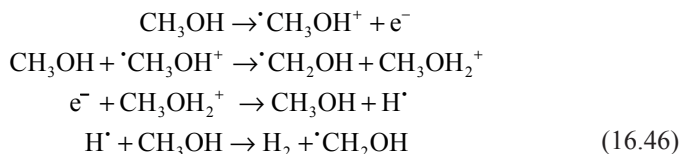
16.4.3.2 Track Structure in Methanol

Several systems were then studied at low dose to determine the point at which spurs and tracks failed to overlap and the spatial distributions were no longer uniform. These were easiest using particles to irradiate the samples rather than X- or γ -rays because the higher concentrations of PCs within particle tracks provided better

Table 16.1 Experimental data on radiation-chemical yields, track radii, and local concentrations in irradiated methanol at 77 K

Radiation source	LET (keV/ μm)	G_R (1/100 eV)	$C_{loc} \times 10^{-18}$ (cm^{-3})	R_{tr} (nm)
β (T)	11	5.5	2.5	9
${}^6\text{Li}(n, \alpha)\text{T}$	160	2.6	7	13
${}^{210}\text{Po}(\alpha)\text{Pb}$	200	3.3	8	15.5
${}^{10}\text{B}(n, \alpha){}^7\text{Li}$	430	1.0	7.5	13
${}^{235}\text{U}(n, f)\text{Pr}$	5400	0.2	7.5	18
β (${}^{35}\text{S}$)	10	6	1.7	9

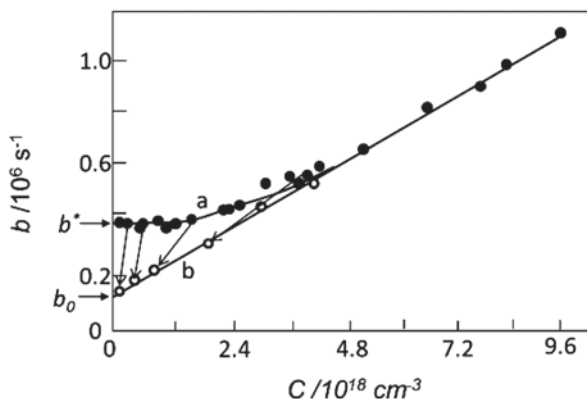
sensitivity. The most detailed studies were carried out for methanol [75–78]. The mechanism of radical formation is well understood in frozen methanol irradiated at 77 K. It is a convenient system for investigation of track effects because it is possible to move radicals from localized tracks to a uniform distribution throughout the volume. The radical formation mechanism in glassy methanol at 77 K is as follows:



Radiation with different linear energy transfer, LET, was used, Table 16.1. Thermal neutron irradiation was carried out in a nuclear reactor. The mean LET for the various sources are included. Small amounts of the corresponding isotopes were dissolved in methanol before freezing as transparent glasses at 77 K, and the echo decay for the CH_2OH radical was investigated. The average radical concentration C_{ave} was determined by CW EPR.

Plots of the echo decay rate b versus the CH_2OH radical C_{ave} during β -irradiation are given in Fig. 16.8 (curve a). At low C_{ave} , b is independent of radical concentration

Fig. 16.8 Concentration dependence of phase relaxation rate of CH_2OH radicals **a** under β -irradiation and **b** after UV photolysis of the irradiated samples. The limiting values of b at $C=0$ are b^* and b_0 for curves **a** and **b** respectively



with a limiting value $b^* = 0.4 \times 10^6 \text{ s}^{-1}$. Above a C_{ave} of about $4 \times 10^{18} \text{ cm}^{-3}$, the decay rate becomes a linear function of concentration for β -irradiation

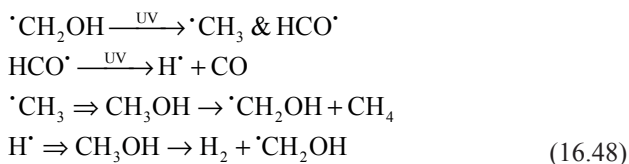
$$b = 0.12 \times 10^6 \text{ s}^{-1} + 1.1 \times 10^{-13} \text{ cm}^3 \text{ s}^{-1} C_{ave} \quad (16.47)$$

The C_{ave} of CH_2OH radicals is linear over the range of absorbed dose and was used to determine the radiation chemical yield G_R in Table 16.1.

Similar experiments were performed with the other types of radiation. The dependence of the echo decay rate on C_{ave} always has the same form characteristic of track spatial inhomogeneity. At small C_{ave} , up to the point of overlapping tracks, the decay rate is constant. With further dose increases, the dependence becomes linear, with the slope expected for a uniform spatial distribution of PCs at the concentration C_{ave} . Only in the case of neutron irradiation was the linear region not observed. The value of $b^* = 0.88 \times 10^6 \text{ s}^{-1}$ was large and the small absorbed dose would not have reached the linear region.

The results of these experiments indicate a non-uniform spatial distribution of radicals. Independent experimental corroboration of such a distribution was obtained by studying the echo decay of the CH_2OH radicals after UV photolysis of the irradiated samples.

It is well known that UV light decomposes CH_2OH radicals into CH_3 , H, and CO [79]. The methyl radicals and hydrogen atoms are unstable in an alcohol matrix at 77 K because they diffuse and react with each other and with the alcohol molecules. This results in the formation of new CH_2OH radicals but with some decrease in their numbers relative to the initial CH_2OH radicals:



The diffusion indicated by the thick arrow must decrease the initial inhomogeneity of their spatial distribution. If irradiated samples are illuminated by UV light and then kept in darkness, the spatial distribution of CH_2OH radicals will be more uniform.

Experiments with UV light exposure were performed as part of the echo decay measurements. Typical results are shown, Fig. 16.8b, for β -irradiation. The arrows show changes in C_{ave} and echo decay rate for CH_2OH radicals in particular samples following UV photolysis and extended storage in darkness. As expected, the echo decay rate became linear with C_{ave} over the entire concentration range and corresponds to a uniform distribution of PCs.

The results allowed one to determine C_{loc} in methanol irradiated by various types of ionizing particles. For a random radical distribution, the dipolar interactions contribute $1.1 \times 10^{-13} \text{ cm}^3/\text{s} C_{ave}$ to the spin echo decay rate, Eq. (16.47). Therefore, for a uniform spatial distribution of radicals inside the tracks, the C_{loc} is given by

$$C_{loc} = \frac{b^* - b_0}{1.1 \times 10^{-13}} \text{ cm}^3 \text{ s} \quad (16.49)$$

Here b^* is the decay rate for C_{ave} (doses) in the initial flat region, Fig. 16.8, where track effects are observed, and b_0 is the y-axis intercept from the linear region. The C_{loc} calculated in this way are listed in Table 16.1.

The geometrical dimensions of the tracks are estimated from C_{loc} . Suppose that the tracks are cylindrical with a radius R_{tr} and a length L equal to the path of the ionizing particle, then

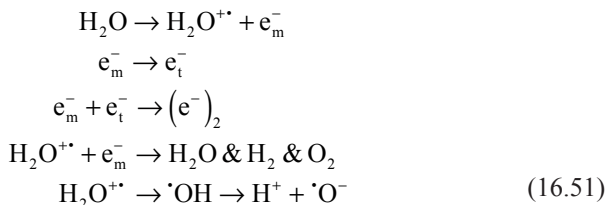
$$R_{tr} = \sqrt{\frac{G_R \cdot LET}{100\pi C_{loc}}} \text{ cm}^3 \text{ s} \quad (16.50)$$

C_{loc} and R_{tr} in methanol irradiated by various types of particles are summarized in Table 16.1. The track structure has been studied by similar methods in other polar compounds irradiated by high-LET particles at low temperatures [75].

16.4.3.3 Detailed Track Structure

The mechanism of CH_2OH radical formation, Eq. (16.46), shows that there are two types of initial damage species produced. One arises from the primary electron. The other from the positive charge or hole, in the case of methanol, the CH_3OH^+ radical cation. But in methanol the electrons and holes produced a single trapped radical product CH_2OH , making it impossible to know the precise origin of the radical being measured. The experiments measure a single mean value for the track radius. Yet, one can argue that radical tracks may have different radii for electron versus hole products if the mobility of their precursors differ, i.e. R_{tr}^- and R_{tr}^+ . This issue was hotly debated in the development of radiation chemistry starting from the early 1950s, for example [80–82]. Detailed track structure from spin echo studies helped resolve the issue.

Two PCs are stabilized in irradiated alkaline glasses at 77 K: trapped electrons (e_t^-) and oxygen radical ions (O^-), produced by a simple sequence of reactions.



Here the t and m subscripts indicate trapped and mobile electrons and $(e^-)_2$ is the di-electron [83, 84]. The spatial distribution of e_t^- is a result of the path length of mobile

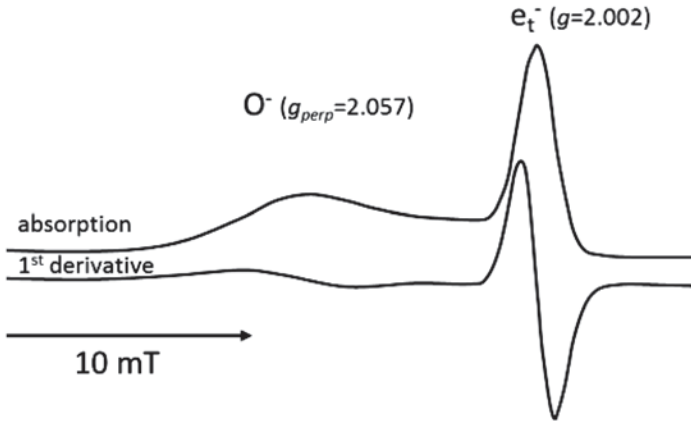


Fig. 16.9 EPR absorption and first-derivative EPR spectra of trapped electrons, e_t^- , and O^- radical ions in γ -irradiated 9M NaOH at 77 K

e_m^- formed in the initial ionization process before they are thermalized and trapped. The O^- radical ions are formed by the last sequence of reactions in Eq. (16.51) which may be preceded by hole transfers from H_2O^+ to H_2O . These reactions allow hole migration through the medium and ultimately determine the spatial distribution of the trapped O^- radical ions. The EPR spectra of O^- and e_t^- overlap negligibly because of the difference in their g -factors, Fig. 16.9. The echo decay of these PCs can be measured separately. Thus there was the possibility to separately study O^- and e_t^- spatial distributions. Frozen solutions of 9 M NaOH were γ -irradiated or doped with small amounts of tritiated water, T_2O , for β -irradiation [85]. The echo decay rate was determined for e_t^- at 77 K and for O^- ion radicals at 77 and 4.2 K.

Instantaneous diffusion is the principal route of echo decay for these PCs. The temperature dependence on the rate for O^- radical ions indicates that it is a ' T_1 '-type sample with $W \leq 10^3 \text{ s}^{-1}$ at 4.2 K. The e_t^- echo decay rate is described by Eq. (16.45) but for O^- by

$$V(\tau) = e^{-2\tau b - a\tau^3} \quad (16.52)$$

The nuclear spin diffusion terms m and a are independent of C_{ave} of the PCs, and the difference in the echo decay kinetics might be caused by different local nuclear environments around e_t^- and O^- . In both cases b depends on p_B and the concentration of PCs. The effect of spatial inhomogeneity was observed only for O^- in β -irradiated samples, Fig. 16.10. The echo decay rates coincide for e_t^- in β - and γ -irradiated samples. The slope of the straight line, Fig. 16.10, gives the value of $\alpha = (6 \pm 2) \times 10^{-13} \text{ cm}^3/\text{s}$, Eq. (16.35), for e_t^- and $7.2 \times 10^{-13} \text{ cm}^3/\text{s}$ for O^- which are close to the theoretical value of $8.2 \times 10^{-13} \text{ cm}^3/\text{s}$ for a uniform distribution of PCs.

The departure from linearity for O^- in β -irradiated samples makes it possible to determine C_{loc} for O^- in a β -track from $b^*/\alpha = 2 \times 10^{18} \text{ cm}^{-3}$, where b^* is the echo decay rate in the region where b is independent of C_{ave} for O^- . Such a C_{loc} corresponds

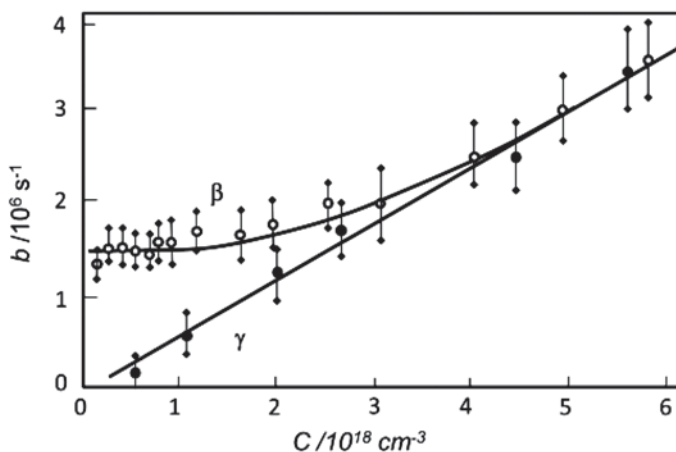


Fig. 16.10 Plots of echo decay rate b vs C_{ave} of O^- radical ions in γ - and β -irradiated samples

to $R_{tr} = 7.5$ nm. The e_t^- are uniformly distributed at least for $C_{ave} > 2 \times 10^{17} \text{ cm}^{-3}$. This value indicates $R_{tr} > 20$ nm for the e_t^- . Thus it is clear that the e_t^- and the O^- radical ions are distributed non-uniformly with respect to each other [85] and have different spatial distributions. Since the mean distance between O^- radical ions in a track is about 7.5 nm, the formation of O^- from H_2O^+ would occur after at least 15 hole transfers.

Frozen glassy solutions of sulfuric and phosphoric acids are also systems in which the detailed structure of radical tracks can be obtained by electron spin echo studies. The e_m^- become trapped as hydrogen atoms after they react with H^+ , and the positively-charged holes react with the acid anions, e.g., SO_4^{2-} , after charge migration, producing the corresponding radical ions (SO_4^-). Behavior of the echo decay for γ -irradiated samples of these acids could be described by a uniform spatial distribution of hydrogen atoms and the radical ions even at the lowest doses that could be studied. Therefore the echo decay rate was studied in α - and β -irradiated solutions of 8 M H_2SO_4 and 12 M H_3PO_4 [86], but we will not describe these studies in detail because the results are similar to those obtained for alkaline glasses. The main results for these systems are summarized in Table 16.2.

The anion PCs resulting from the positively charged H_2O^+ holes are localized in a region with a radius of about 7 nm, while the trapped electrons or hydrogen atoms, with mobile electrons as precursors, are localized in much larger volumes with radii exceeding 20 nm.

It is much more difficult to distinguish electron and hole products in organic matrices because the products are PCs with very similar, overlapping spectra or, as in the case of methanol, Eq. (16.46), the products are identical. The use of electron scavengers can allow determination of the spatial distribution of electron and hole products. The β -radiolysis of 1 M solutions of cadmium perchlorate $Cd(ClO_4)_2$ in methanol results in two types of PCs: Cd^+ ions with mobile or trapped electrons as precursors

Table 16.2 Radiation-chemical yields, local concentrations, and track radii in methanol and in aqueous acid and alkaline solutions irradiated at 77 K

Solution	PC	Radiation	G_R (1/100 eV)	$C_{loc} \times 10^{-17}$ (cm ⁻³)	R_{tr} (nm)
8 M H ₂ SO ₄	H	$\beta(^3\text{H})$	2.0	<2	>20
	H	$\alpha(^{110}\text{Po})$	0.85	~10	~25
	SO ₄ ⁻	$\beta(^3\text{H})$	2.0	15	6.5
	SO ₄ ⁻	$\alpha(^{110}\text{Po})$	1.7	120	10
12 M H ₃ PO ₄	H	$\alpha(^{110}\text{Po})$	0.46	~4	~30
	PO ₄ ⁻	$\alpha(^{110}\text{Po})$	1.1	110	8.5
8 M NaOH	e _t ⁻	$\beta(^3\text{H})$	2.7±0.3	<2	>20
	O ⁻	$\beta(^3\text{H})$	3.7±1	20	7.5
Methanol	Cd ⁺	$\beta(^3\text{H})$		25	>13
	holes	$\beta(^3\text{H})$		25	2.5

and CH₂OH radicals with CH₃OH⁺ as precursors. Their EPR spectra overlap only partially. Cd⁺ has an asymmetric doublet that overlaps the CH₂OH radical spectrum but is approximately six times more intense. The low-field portion of the CH₂OH spectrum is free of overlap. It is possible to make echo decay measurements for each PC due to the large differences in their EPR signal intensities at different fields.

Within experimental error of 30–40%, in β - or γ -irradiated samples, equal amounts of Cd⁺ and CH₂OH are formed with radiation-chemical yields of 2.5×10^{-2} eV⁻¹ in β -irradiated and 3×10^{-2} eV⁻¹ in γ -irradiated samples [87]. The dipolar interactions, the local concentrations and the track radii were determined for each PC from the echo decay rates. Measurements in the β -irradiated samples were made at 4.2 K at concentrations of 10^{17} – 10^{19} cm⁻³. The echo decay kinetics for both PCs is described by Eq. (16.45) for uniform distributions of paramagnetic centers. But in contrast to systems that really have a uniform distribution, the decay rate for CH₂OH in β -irradiated samples is constant up to $C_{ave} \sim 2.5 \times 10^{18}$ cm⁻³. For larger C_{ave} , the decay becomes linear with C_{ave} ; with the same slope obtained for uniform CH₂OH distribution. The hole products are trapped in spatially restricted regions—the tracks of ionizing particles with $R_{tr} = 2.5$ nm in β -irradiated methanol. The local concentration of Cd⁺ ions is apparently so low that the dipolar interaction for their track cannot be measured. Estimations of the minimum radius gives $R_{tr} > 13$ nm for the electron products in methanol. These results may be considered a direct verification of models for the structure of ionizing particle tracks in condensed phases that were put forward as far back as 1951 by Lea, Gray, and Platzman [80, 81].

16.4.3.4 Ammonium Tartrate

Instantaneous diffusion of X-irradiated single crystals and powders of ammonium tartrate was studied at room temperature by Brustolon et al. [88]. Irradiated ammonium tartrate has a single long-lived free radical with rather slow relaxation rates at room temperature and has been proposed as a convenient chemical dosimeter. The

rate of echo decay by instantaneous diffusion was exponential and k_{ID} of Eq. (16.35) for different radiation doses was measured by varying p_B . A straight line was fit to a plot of k_{ID} versus radical concentration in single crystals and the distribution of radicals was concluded to be uniform. An extension of this work discussed later in Sect. 16.5.3 found that at lower doses, k_{ID} is constant and corresponds to the C_{loc} of isolated ionization events. If a line going through the origin, consistent with Eq. (16.35) is drawn through the data, then a break appears at low dose similar to those discussed for non-uniform distributions.

Measurements were also made on ammonium tartrate powder at doses above the apparent break in the single crystal response. Again, the k_{ID} could be fit by a straight line that did not pass through the origin. The scatter in the points is much less than for single crystal samples and it is clear that the data is incompatible with a uniform distribution in Eq. (16.35). The empirical data does support the suggestion by Brustolon et al. [88] to measure radical concentration and hence dose from the rate of instantaneous diffusion in powders rather than by quantitative EPR.

16.4.3.5 Other Approaches

Ichikawa et al. [89–91] examined several γ -irradiated solids. Cross relaxation between PCs was extrapolated to zero dose to estimate the cross relaxation between PCs within the same spur. Average local concentrations and spur sizes were consistent with those found by the Kevan group using CW EPR and discussed in Sect. 16.3.3.

The determination of the tail of f_{pc} for PC pairs produced by photolysis [92, 93] or γ -radiation [94] was reviewed by Raitsimring and Salikhov [3]. Metal ions were photolyzed or sulfuric acid solutions were irradiated to produce a free radical trapped near a fast-relaxing PC, creating ‘ T_1 ’ spectral diffusion. The tail of f_{pc} extending beyond 1.7 nm was determined and diffusion of hydrogen atoms during thermal annealing was observed. W_B of the metal ions was too small to enable observation of pairs with distances any smaller than 1.7 nm.

16.4.3.6 Summary

In several studies mentioned here, the kinetics of the echo decay had the form expected for a uniform spatial distribution of PCs, while variation of the dose and C_{ave} indicated an inhomogeneous distribution at low doses. This apparent contradiction arises because of the small window of distances that contribute to the observed decay. One can expect that within the spur or track radius, the f_{pc} is fairly constant and corresponds to the C_{loc} derived from the instantaneous diffusion. There is good consistency among the number of PCs in the sample, C_{loc} and the size of the tracks. PCs formed by low-mobility holes lie in a track with radii of 2.5 nm (frozen methanol) to 8.5 nm (frozen acid glasses) around the path of β -particles. Electrons or mobile hydrogen atoms in the same samples have track radii at least 13–30 nm.

Much of the uncertainty in the size of the track of electron products results from the low doses necessary for their measurement and the limited sensitivity of pulsed EPR spectrometers when the measurements were made.

16.5 Pulsed Dipolar Spectroscopy

The spin echo based measurements of distance distributions discussed in Sect. 16.4 are a major advance over CW measurements because refocusing of inhomogeneous broadening allows more precise measurement of dipolar interactions. Yet, a number of other effects still are present in the intrinsic echo decay $V_{int}(T_M, \tau)$ of Eq. (16.29). V_{int} is often a non-exponential or even non-monotonic decay that must be separated from V_{SD} based on variation of the decay with dose, temperature or p_B . Errors in separating these two contributions to the total echo decay propagate into f_{pc} .

Just as the spin echo is able to ‘refocus’ inhomogeneous broadening, pulse sequences for pulsed dipolar spectroscopy, PDS, ‘refocus’ the intrinsic decay that is unrelated to dipolar interactions. Most PDS methods belong to a class of constant time measurements in which an echo is measured, but delay times, such as τ and T , are kept constant so that V_{int} remains constant. One family of techniques has its roots in double resonance spectroscopy [13] while the other is known as double quantum coherence or DQC spectroscopy [95].

16.5.1 DEER

The most common electron double resonance experiment, known as DEER or PELDOR [13, 49, 96–98], uses two different microwave frequencies while a variant known as the ‘2+1’ sequence uses only one frequency [47]. They are, in fact, two limiting cases of the same technique. The ‘2+1’ sequence is suited for measurements on a single type of PC with a narrow EPR spectrum while DEER is ideal for two kinds of PCs with very different EPR spectra.

The three-pulse DEER experiment generates a spin echo from A spins using a pair of pulses at one microwave frequency, ω_A , with a fairly large τ . A pulse at a second microwave frequency, ω_B , is applied at a time τ' between the two detection pulses, Fig. 16.3c. In the simple model of DEER with $W_B=0$, the detection pulses only excite A spins while the pump pulse only excites B spins. The intrinsic decay V_{int} of the A spins does attenuate the echo, but does not change during a DEER measurement with constant τ . For $\tau'=0$, the dipolar interaction between A and B spins is refocused, but as τ' increases from 0 to τ , the dipolar interaction suddenly shifts the EPR frequency of the A spins, causing abrupt ‘instantaneous’ spectral diffusion.

$$V(\tau) = V_{int}(T_M, \tau) V_{Dip}(\tau')$$

$$\langle V(\tau) \rangle \approx \langle V_{int}(T_M, \tau) \rangle \langle V_{Dip}(\tau') \rangle \quad (16.53)$$

Virtually every analysis of DEER data is based on the ability to factor the dipolar response, and its averages, from all other effects, Eq. (16.53). The dipolar interaction impacts the signal only during τ' , as V_{Dip} , while the intrinsic decay V_{int} is totally independent of dipolar interactions and occurs only during τ . The echo intensity for an A spin interacting with several B spins is related to $V_{\text{pair,B}}$ of Eq. (16.31).

$$V_{\text{Dip}}(\tau') = \prod_i V_{\text{pair,B}_i}(\tau') \quad (16.54)$$

The same averaging in Eqs. (16.33–16.39) for instantaneous diffusion applies as long as V_{int} does not depend on dipolar interactions and Eq. (16.53) holds. There is a four-pulse variant of DEER, Fig. 16.3d, that overcomes practical problems when two microwave pulses overlap at $\tau'=0$ [99].

This simple model provides an easily-understood picture of how DEER works and why distance distributions can be derived from it. Unfortunately this simple model often does not correspond to the actual experiment. The detection pulses typically excite B spins and the pump pulse excites A spins. These possibilities have long been recognized in ‘2+1’ measurements [46, 47] where the pump and detection pulses have the same frequency, but have just been considered in detail for three-pulse DEER [52] and remain to be dealt with in four-pulse DEER.

When the second detection pulse at ω_A excites B spins, the DEER response depends not just on $\cos(D\tau')$, but also on $\cos(D\tau)$ and $\cos(D(\tau-\tau'))$ [52]. This last term is significant only when the B spin is excited by pulses at both frequencies. This term may be neglected under normal conditions when the difference of the two mw frequencies is large compared to the mw field strength. Then the $\cos(D\tau')$ term may be recovered as $\cos(D\tau') = [V(\tau') - V(\infty)]/[V(0) - V(\infty)]$. In general, even if τ is constant during a measurement, the DEER signal cannot be separated, as implied in Eq. (16.53), into a V_{int} term independent of dipolar couplings and a V_{Dip} term depending only on dipolar-driven spectral diffusion during τ' . A partial solution to this problem lies in the careful selection of pump and detection parameters [100] or having p_A and $p_B \ll 1$ for A and B spins for both ω_A and ω_B . However, unless $W\tau \ll 1$, B spin relaxation and flip-flops still prevent the clean separation of terms in Eq. (16.53) [52].

16.5.1.1 Uniform Distribution

Equation (16.53) applies in the limit of $W \sim 0$ and with selective pump and detection pulses that only excite the desired PCs, and the DEER signal in Eq. (16.54) has the same form as Eq. (16.34) for instantaneous diffusion if τ is replaced by τ' . Equation (16.54) allows the DEER decay to be broken into products of decays from conveniently chosen sets of PCs. The distinction often made for instantaneous diffusion studies is quite appropriate: a background decay from a uniform distribution of B spins belonging to different spurs or tracks and a decay from B spins within the same spur or track. The uniform distribution of B spins produces an exponential

decay in Eq. (16.35). The decay rate is proportional to p_B and can be made arbitrarily slow, but the DEER signal decays smoothly to zero.

The DEER decay is derived from averages of $\cos(D\tau')$ which is symmetrical around $\tau'=0$. The decay in a four-pulse DEER from a uniform distribution is also symmetric and should have a peak with a sharp corner at $\tau'=0$. Any departure from a uniform distribution at short distances caused by excluded volume [101], recombination or tunneling will round off this peak and make it smoother, but still symmetric. This part of the decay can be experimentally measured with DEER but it is lost in the deadtime in spin echo measurements. DEER has much smaller deadtime because the pump pulse can be placed adjacent to the detection pulses in three-pulse DEER for a deadtime of approximately the pulsewidth, while four-pulse DEER lacks even this restriction. The smallest values of τ' provide data on the largest dipolar interactions and the shortest PC separation distances. A number of reviews consider the DEER decay from free radicals distributed uniformly in various dimensions [13, 49, 98] which may be relevant to damage at surfaces or to extended polymers.

16.5.1.2 Within the Track or Spur

The decay from PCs within the same spur or track is given by the same averages as for $\langle V_{ID} \rangle$, Eqs. (16.38 and 16.39), which require p_A and $p_B \ll 1$. An important advantage of DEER relative to instantaneous diffusion measurements is the lack of deadtime which can reveal the initial decay in Eq. (16.39) that is important for determining the number of PCs in the spur and the dipolar second moment. This is the same distance range where the uniform distribution assumption fails. Fortunately it is possible to disentangle them because the intra-spur or track contributions to the DEER decay are independent of dose while the contribution from PCs in different spurs or tracks depends linearly with dose, at least initially.

DEER has been applied to the determination of PC cluster sizes and spatial distributions in several areas including radiation chemistry, structural biology and polymers. A critical examination of both abilities was made using a series of bi-, tri-, and tetra-radicals by Bode et al. [101]. Counting the number of PCs in a cluster rests on the difference in DEER decay for a finite cluster versus a uniform distribution. The cluster has a decay rate that is not linear with p_B and the DEER intensity for small p_B reaches a non-zero limiting value at long τ' [13, 102]. Bode et al. [101] successfully counted the number of radicals when only a single compound was present. In mixtures of mono- through tetra-radicals, average numbers of spins per radical were obtained for DEER data with high signal to noise ratios.

In multi-radicals, each pair of spins produces DEER modulation and the distance between spins can be determined at low p_B . The relative amplitudes for different inter-spin distances did not match the structure of the multi-radicals [101] and was ascribed, in part, to the use of analysis software designed only for pairs of PCs. This study has some relevance to measurement of f_{pc} for systems with more than pairs of PCs and it does support an earlier measurement of multiple inter-spin distances by Bowman et al. [103] in end-to-end stacks of spin-labelled RNA duplexes.

16.5.2 DQC

Double Quantum Coherence spectroscopy or DQC [104, 105] uses a double quantum filter to ensure that only the dipolar evolution of PCs is measured. In its usual implementation, DQC uses a single microwave frequency and requires the PCs to have relatively narrow EPR spectra. One advantage relative to DEER is that there is no signal background from isolated PCs, which have no double quantum coherence. DQC works well with pairs of PCs, but larger clusters would appear to produce responses with sums and differences of dipolar interactions. These combinations of dipolar interactions are suppressed in instantaneous diffusion and DEER measurements in the $p_B \ll 1$ limit, but this remedy does not seem to be practical in DQC. However, development of rigorous filtering and rejection of higher-order coherences may make such techniques applicable beyond the realm of pairs of PCs.

16.5.3 Experimental Studies

One of the first applications of DEER was the study of semiquinone radical—deuterium atom pairs formed by photolysis of hydroquinone in frozen solutions of deuterated sulfuric acid [106]. The deuterium atom was rapidly thermalized and trapped in close proximity to the semiquinone radical. Strong DEER signals indicated pairs of PCs relatively isolated from each other. The f_{pc} was extracted from this data in the original paper [106] and later by a more exact procedure [107]. The f_{pc} in both analyses has a peak near 4 nm with a shoulder between 6 and 9 nm before tailing to zero at long distances. The f_{pc} falls sharply to zero at distances less than about 1.5 nm.

Kurshev et al. [46] used the ‘2+1’ sequence (DEER with only one microwave frequency) to determine the distribution of pairs of hydroxyalkyl radicals produced by photolysis of frozen acidic solutions of deuterated alcohols. They obtained good fits to the data for a f_{pc} proportional to $\exp[-(r/r_c)^6]$ for a set of alcohols with 1–4 carbons. The value of r_c ranged from 6.5 to 7.2 nm across these alcohols. This f_{pc} is roughly a uniform distribution to r_c where it drops to zero. The r_c determined by the ‘2+1’ sequence are 0.6–1.3 nm larger than those measured in γ -irradiated protiated alcohols by Ichikawa et al. [90] using a cross relaxation method. It is significant that both sets of data were fit with the same functional form of f_{pc} . This relatively flat f_{pc} seems consistent with the uniform distributions found in instantaneous diffusion measurements where the decays were primarily caused by PCs at distances shorter than r_c .

DEER was used by Bowman et al. [108] to probe the spatial distribution of PCs in DNA irradiated at 77 K to doses of 1.7–50 kGy by heavy-ion beams of 100 MeV per nucleon ^{40}Ar ions having an LET of 300–400 keV/ μm . These ions produce dense tracks of damage in their wake with extensive recombination of PCs. At these doses, the tracks are well separated from each other and the samples had superimposable DEER spectra. Smoothly-decaying DEER spectra were measured over

a range of p_B that varied by a factor of 12. At the smaller values of p_B , the signal intensity reached an asymptotic value that allowed determination of the number N of PCs contributing to the DEER decay. The rate at which it approached the asymptote gave the local concentration of those PCs. Unfortunately, p_B was incorrectly calculated and is underestimated, leading to an overestimation of N and local concentration. This error is partly offset when the track radius is calculated. A global fit of all samples and data reported $N \sim 18$, $C_{loc} \sim 13.5 \times 10^{19}$ PC cm⁻³ and a track radius of 6.8 nm. These numbers were consistent with the known LET and radiation chemical yield.

Marrale et al. [109] extended the instantaneous diffusion study of irradiated polycrystalline ammonium tartrate with a study that includes DEER and γ -, neutron- and 19.3 MeV proton-irradiation. A careful examination of k_{ID} following up [88] for each radiation type ensured that the DEER reflected spatial distribution of a single ionization event. This appears to be the first case reported of DEER decays in irradiated materials showing pronounced modulation that was not traced to nuclear modulation (ESEEM) artifacts [98]. The resolved modulation was assigned to radicals being trapped at the sites of molecules within the crystal structure. Unfortunately, these remarkable DEER spectra were not shown. The f_{pc} extracted from the DEER data lies almost entirely between 2.0 and 5.5 nm with ripples corresponding to translations of the unit cell. This distribution was reproduced very closely by detailed simulations incorporating the crystal structure and anisotropic recombination. The observed and simulated differences in PC distribution with different types of radiation were suggested as providing a way to determine LET of unknown radiation by using the ammonium tartrate dosimeter.

16.6 Future Prospects

The main advantage of pulsed EPR is the removal of the inhomogeneous broadening of EPR lines and the removal of decay not caused by dipolar interactions. This reveals the dipolar width and, therefore, opens new possibilities to detect non-uniform spatial distribution of PCs in radical tracks and spurs. The two-pulse ESE is the simplest and most direct experimental approach to these problems but DEER holds greater potential.

The two-pulse spin echo spectroscopy has its limitations. In analyzing ESE data in order to get dipolar broadening, it is necessary to subtract the other relaxations and spin dynamics effects that appear in the two-pulse echo decay, such as spectral diffusion, nuclear-spin diffusion and ESEEM. This is not a simple task as one pushes sensitivity to probe large structures. DEER provides a much cleaner signal free from many of the competing decays, but at the price of a significant loss of sensitivity. Fortunately sensitivity continually increases as a result of advances in microwave and magnet technology coupled with digital control and data acquisition. Many of these advances are now being driven by the use of DEER in structural biology where spectacular sensitivity has been achieved with high-field pulsed EPR.

Currently, the theoretical basis to extract spatial distributions from DEER has significant gaps, particularly for treating the higher-order correlations needed in spectral diffusion of ' T_2 '-samples and for extracting f_{pc} when there is more than a single pair of PCs involved. But both issues affect the application of DEER in fields beyond radiation chemistry. Likewise, the spatial distribution of PCs is often correlated with the spatial inhomogeneity of the sample and may be a major opportunity for new applications of pulsed EPR studies. The interaction of plasmas with surfaces and nanomaterials; radiation chemistry at interfaces; and the distribution of electrons and holes in nanoparticles used for energy conversion provide new challenges and opportunities that can be addressed by well-designed EPR studies.

References

1. Salikhov KM, Semenov AG, Tsvetkov YD (1976) Electron spin echoes and their applications. Nauka, Novosibirsk
2. Salikhov KM, Tsvetkov YD (1979) Electron spin echo studies of spin-spin interactions in solids. In: Kevan L, Schwartz RN (eds) Time domain electron spin resonance. Wiley, New York, pp 231–278
3. Raitsimring AM, Salikhov KM (1985) Electron spin echo method as used to analyze the spatial distribution of paramagnetic centers. Bull Magn Reson 7(4):184–217
4. Weil JA, Bolton JR, Wertz JE (2007) Electron paramagnetic resonance elementary theory and practical applications, 2nd edn. Wiley-Interscience, New York
5. Schweiger A, Jeschke G (2001) Principles of pulse electron paramagnetic resonance. Oxford University Press, Oxford
6. Bowman MK (2011) Pulsed methods in electron spin resonance. In: Meyers RA (ed) Encyclopedia of analytical chemistry, vol S1–S3. Wiley, Chichester, pp 1548–1572
7. Brustolon M, Giannello E (2009) Electron paramagnetic resonance—a practitioner's toolkit. Wiley, Hoboken
8. Bedilo AF, Maryasov AG (1995) Electron spin resonance of dipole-coupled anisotropic pairs in disordered systems. Secular approximation for point dipoles. J Magn Reson Ser A 116:87–96
9. Abragam A, Bleaney B (1986) Electron paramagnetic resonance of transition ions. Dover, New York
10. Maryasov AG, Bowman MK, Tsvetkov YD (2006) Dipole-dipole interactions of high-spin paramagnetic centers in disordered systems. Appl Magn Reson 30(3–4):683–702
11. Abragam A (1961) The principles of nuclear magnetism. The international series of monographs on physics. Clarendon, Oxford
12. Yudanov VF, Salikhov KM, Zhidomirov GM, Tsvetkov YD (1969) Modulation effects in the electron spin echo of biradical systems. Teor Eksp Khim 5:663–668
13. Milov AD, Maryasov AG, Tsvetkov YD (1998) Pulsed electron double resonance (PELDOR) and its applications in free-radicals research. Appl Magn Reson 15(1):107–143
14. Jeschke G (2002) Determination of the nanostructure of polymer materials by electron paramagnetic resonance spectroscopy. Macromol Rapid Comm 23(4):227–246. doi:10.1002/1521-3927(20020301)23:4<227::Aid-Marc227>3.0.Co;2-D
15. Weber A, Schiemann O, Bode B, Prisner TF (2002) PELDOR at S- and X-band frequencies and the separation of exchange coupling from dipolar coupling. J Magn Reson 157(2):277–285. doi:10.1006/jmre.2002.2596
16. Pshchetskii SY, Kotov AG, Milinchuk VK, Roginskii VA, Tupikov VI (1974) EPR of free radicals in radiation chemistry. Halsted Press, New York

17. Kurita Y (1964) Electron spin resonance study of radical pairs trapped in irradiated single crystals of dimethylglyoxime at liquid-nitrogen temperature. *J Chem Phys* 41(12):3926–3927. doi:10.1063/1.1725837
18. Gordy W, Morehouse R (1966) Triplet-state electron spin resonance of an H-atom-methyl-radical complex in a solid matrix. *Phys Rev* 151(1):207–210. doi:10.1103/PhysRev.151.207
19. Lebedev YS (1966) Radical pairs in photolytic decomposition of azobisisobutyronitril as investigated by ESR method. *Dokl Akad Nauk SSSR* 171(2):378–381
20. Steinhoff HJ (2004) Inter- and intra-molecular distances determined by EPR spectroscopy and site-directed spin labeling reveal protein-protein and protein-oligonucleotide interaction. *Biol Chem* 385(10):913–920. doi:10.1515/Bc.2004.119
21. Rabenstein MD, Shin YK (1995) Determination of the distance between 2 spin labels attached to a macromolecule. *Proc Natl Acad Sci U S A* 92(18):8239–8243. doi:10.1073/pnas.92.18.8239
22. Vincow G, Johnson PM (1963) Second moments of electron spin resonance proton hyperfine spectra. *J Chem Phys* 39(5):1143–1153. doi:10.1063/1.1734404
23. Bales BL, Helbert J, Kevan L (1974) Electron-paramagnetic resonance and electron-nuclear double resonance line shape studies of trapped electrons in gamma-irradiated deuterium-substituted 10 M sodium-hydroxide alkaline ice glass. *J Phys Chem* 78(3):221–231. doi:10.1021/J100596a006
24. Mikhailov AI, Lebedev YS (1967) Evaluation of local concentrations of free radicals in irradiated solids from the change in the EPR line widths. *Khimiya Vysokikh Energii* 1(4):397–399
25. Castner TG (1959) Saturation of the paramagnetic resonance of a V-center. *Phys Rev* 115(6):1506–1515. doi:10.1103/PhysRev.115.1506
26. Portis AM (1953) Electronic structure of *F* centers: saturation of the electron spin resonance. *Phys Rev* 91(5):1071–1078
27. Kevan L, Kispert LD (1976) *Electron spin double resonance spectroscopy*. Wiley, New York
28. Weger M (1960) Passage effects in paramagnetic resonance experiments. *Bell Labs Tech J* 39(4):1013–1112
29. Thomas DD, Dalton LR, Hyde JS (1976) Rotational diffusion studied by passage saturation transfer electron-paramagnetic resonance. *J Chem Phys* 65(8):3006–3024. doi:10.1063/1.433512
30. Sczaniecki PB, Hyde JS, Froncisz W (1990) Continuous wave multi-quantum electron-paramagnetic resonance spectroscopy. *J Chem Phys* 93(6):3891–3898. doi:10.1063/1.458775
31. Zimbrick J, Kevan L (1966) Paramagnetic relaxation of trapped electrons in irradiated alkaline ices. *J Am Chem Soc* 88(15):3678–3679. doi:10.1021/Ja00967a059
32. Zimbrick J, Kevan L (1967) Paramagnetic relaxation of trapped electrons in irradiated alkaline ices. *J Chem Phys* 47(7):2364–2371. doi:10.1063/1.1703319
33. Zimbrick J, Kevan L (1967) Paramagnetic relaxation of trapped hydrogen atoms in irradiated frozen aqueous solutions. *J Chem Phys* 47(12):5000–5008. doi:10.1063/1.1701751
34. Zimbrick J, Kevan L (1967) Paramagnetic relaxation of trapped hydrogen atoms in irradiated frozen solutions. *Nature* 214(5089):693. doi:10.1038/214693a0
35. Hase H, Kevan L (1969) Paramagnetic relaxation of radiation-produced electrons in annealed glassy and polycrystalline alkaline ices. *J Phys Chem* 73(10):3290–3293. doi:10.1021/J100844a024
36. Chen DH, Kevan L (1969) Paramagnetic relaxation of trapped electrons in gamma-irradiated organic glasses. *Mol Cryst Liq Cryst* 9:183–196. doi:10.1080/15421406908082738
37. Bales BL, Kevan L (1970) Paramagnetic relaxation of silver species in gamma-irradiated frozen aqueous solutions. *J Chem Phys* 52(9):4644–4653. doi:10.1063/1.1673697
38. Lin DP, Kevan L (1971) Paramagnetic relaxation study of spatial distribution of trapped electrons in gamma-irradiated organic glasses. *J Chem Phys* 55(6):2629–2635. doi:10.1063/1.1676470

39. Lin DP, Kevan L, Hamlet P (1972) Paramagnetic relaxation study of spatial-distribution of trapped radicals in gamma irradiated alkaline ice and organic glasses at 4.2 degrees K. *J Phys Chem* 76(8):1226–1227. doi:10.1021/J100652a024
40. Lin DP, Kevan L (1972) Optical bleaching effects on paramagnetic relaxation of trapped electrons in methyltetrahydrofuran at 77 degrees K. *J Phys Chem* 76(5):636–639. doi:10.1021/J100649a004
41. Hase H, Feng DF, Bowman MK, Kevan L (1975) On the applicability of slow passage EPR relaxation theories to saturation curves for trapped electrons in organic glasses. *Chem Phys Lett* 30(2):204–207
42. Hahn EL (1950) Spin echoes. *Phys Rev* 80(4):580–594
43. Mims WB (1972) Electron spin echoes. In: Geschwind S (ed) *Electron paramagnetic resonance*. Plenum, New York, pp 263–352
44. Klauder JR, Anderson PW (1962) Spectral diffusion decay in spin resonance experiments. *Phys Rev* 125(3):912–932. doi:10.1103/PhysRev.125.912
45. Salikhov KM, Dzuba SA, Raitsimring AM (1981) The theory of electron spin-echo signal decay resulting from dipole-dipole interactions between paramagnetic centers in solids. *J Magn Reson* 42(2):255–276
46. Kurshev VV, Raitsimring AM, Ichikawa T (1991) Spatial-distribution of free-radicals in gamma-irradiated alcohol matrices determined by the 2+1 electron-spin echo method. *J Phys Chem* 95(9):3564–3568. doi:10.1021/J100162a025
47. Kurshev VV, Raitsimring AM, Tsvetkov YD (1989) Selection of dipolar interaction by the 2+1 pulse train ESE. *J Magn Reson* 81(3):441–454
48. Mims WB (1972) Envelope modulation in spin-echo experiments. *Phys Rev B-Solid St* 5(7):2409–2419. doi:10.1103/PhysRevB.5.2409
49. Tsvetkov YD, Milov AD, Maryasov AG (2008) Pulse electron-electron double resonance (PELDOR) as nanometre range EPR spectroscopy. *Usp Khim* 77(6):515–550
50. Abramowitz M, Stegun IA (1964) *Handbook of mathematical functions with formulas, graphs, and mathematical tables*. U.S. Govt. Print. Off., Washington, DC
51. Mims WB, Nassau K, Mcgee JD (1961) Spectral diffusion in electron resonance lines. *Phys Rev* 123(6):2059–2069. doi:10.1103/PhysRev.123.2059
52. Salikhov KM, Khairuzhdinov IT, Zaripov RB (2014) Three-pulse ELDOR theory revisited. *Appl Magn Reson* 45(6):573–619. doi:10.1007/s00723-014-0541-7
53. Raitsimring AM, Salikhov KM, Umanskii BA, Tsvetkov YD (1974) Instantaneous diffusion in electron-spin echo of paramagnetic centers stabilized in solid matrices. *Fiz Tverd Tela* 16(3):756–766
54. Hartmann SR, Hu P (1974) Theory and support for an uncorrelated-sudden-jump model of spectral diffusion decay. *J Magn Reson* 15(2):226–233. doi:10.1016/0022-2364(74)90074-2
55. Hu P, Hartmann SR (1974) Theory of spectral diffusion decay using an uncorrelated-sudden-jump model. *Phys Rev B* 9(1):1–13. doi:10.1103/Physrevb.9.1
56. Bloch F (1946) Nuclear induction. *Phys Rev* 70(7-8):460–474
57. Mims WB (1968) Phase memory in electron spin echoes lattice relaxation effects in CaWO_4 -Er, Ce, Mn. *Phys Rev* 168(2):370–389. doi:10.1103/PhysRev.168.370
58. Brown IM (1979) Electron spin echo studies of relaxation processes in molecular solids. In: Kevan L, Schwartz RN (eds) *Time domain electron spin resonance*. Wiley, New York, pp 195–229
59. Kulik LV, Dzuba SA, Grigoryev IA, Tsvetkov YD (2001) Electron dipole-dipole interaction in ESEEM of nitroxide biradicals. *Chem Phys Lett* 343(3-4):315–324. doi:10.1016/S0009-2614(01)00721-7
60. Savitsky A, Dubinskii AA, Flores M, Lubitz W, Mobius K (2007) Orientation-resolving pulsed electron dipolar high-field EPR spectroscopy on disordered solids: I. Structure of spin-correlated radical pairs in bacterial photosynthetic reaction centers. *J Phys Chem B* 111(22):6245–6262. doi:10.1021/Jp070016c
61. Milikisyants S, Scarpelli F, Finiguerra MG, Ubbink M, Huber M (2009) A pulsed EPR method to determine distances between paramagnetic centers with strong spectral anisotropy and

- radicals: the dead-time free RIDME sequence. *J Magn Reson* 201(1):48–56. doi:10.1016/j.jmr.2009.08.008
62. Astashkin AV, Elmore BO, Fan WH, Guillemette JG, Feng CJ (2010) Pulsed EPR determination of the distance between Heme iron and FMN centers in a human inducible nitric oxide synthase. *J Am Chem Soc* 132(34):12059–12067. doi:10.1021/ja104461p
 63. Savitsky A, Dubinskii AA, Zimmermann H, Lubitz W, Mobius K (2011) High-field dipolar electron paramagnetic resonance (EPR) spectroscopy of nitroxide biradicals for determining three-dimensional structures of biomacromolecules in disordered solids. *J Phys Chem B* 115(41):11950–11963. doi:10.1021/Jp206841v
 64. Milikisyants S, Scarpelli F, Finiguerra M, Ubbink M, Huber M (2011) Distances between paramagnetic metal centers and spin labels in proteins by pulsed EPR: the RIDME method as a new tool. *Biophys J* 100(3):143–143
 65. Zaripov RB, Dzhabarov VI, Knyazev AA, Galyametdinov YG, Kulik LV (2011) Use of additional fast-relaxing paramagnetic species for improvement of RIDME performance. *Appl Magn Reson* 40(1):11–19. doi:10.1007/s00723-010-0170-8
 66. Astashkin AV, Rajapakshe A, Cornelison MJ, Johnson-Winters K, Enemark JH (2012) Determination of the distance between the Mo(V) and Fe(III) Heme centers of wild type human sulfite oxidase by pulsed EPR spectroscopy. *J Phys Chem B* 116(6):1942–1950. doi:10.1021/Jp210578f
 67. Savitsky A, Niklas J, Golbeck JH, Mobius K, Lubitz W (2013) Orientation resolving dipolar high-field EPR spectroscopy on disordered solids: II. Structure of spin-correlated radical pairs in photosystem I. *J Phys Chem B* 117(38):11184–11199. doi:10.1021/Jp401573z
 68. Konov KB, Knyazev AA, Galyametdinov YG, Isaev NP, Kulik LV (2013) Selective hole-burning in RIDME experiment: dead-time free measurement of dipolar modulation. *Appl Magn Reson* 44(8):949–966. doi:10.1007/s00723-013-0464-8
 69. Kulikov AV, Likhtenstein GI (1977) The use of spin relaxation phenomena in the investigation of the structure of model and biological systems by the method of spin labels. *Adv Mol Relax Interact Process* 10(1):47–79
 70. Likhtenshtein GI (2000) Depth of immersion of paramagnetic centers in biological systems. In: Berliner LJ, Eaton GR, Eaton SS (eds) *Distance measurement in biological systems by EPR. Biological magnetic resonance*, vol 19. Kluwer, New York, pp 309–345
 71. Bowman MK, Norris JR (1982) Cross relaxation of free radicals in partially ordered solids. *J Phys Chem* 86(17):3385–3390
 72. Milov AD, Salikhov KM, Tsvetkov YD (1972) Spin-lattice relaxation of hydrogen-atoms and paramagnetic ions in glassy aqueous-solutions of sulfuric-acid at 77 degrees K. *Fiz Tverd Tela* 14(8):2211–2215
 73. Milov AD, Salikhov KM, Tsvetkov YD (1972) Spin diffusion and kinetics of spin-lattice relaxation of hydrogen-atoms in glassy matrices at 77 degrees K. *Fiz Tverd Tela* 14(8):2259–2264
 74. Milov AD, Salikhov KM, Tsvetkov YD (1973) Spin diffusion and kinetics of spin-lattice relaxation of hydrogen-atoms in glassy matrices at 77 degrees K. *Fiz Tverd Tela* 14(8):1956–1960
 75. Raitsimring AM, Moralev VM, Tsvetkov YD (1973) Spatial distribution and yields of radicals formed under the action of radiations with LET of 1–600 eV/A in certain polar compounds. *Khimiya Vysokikh Energii* 7(2):125–128
 76. Raitsimring AM, Pomytkin AP, Tsvetkov YD (1970) Space distribution of radicals during g-irradiation of methanol at 77 K. *Khi Vys Energ* 4(4):369–370
 77. Tsvetkov YD, Raitsimring AM (1970) Electron spin echo technique for spatial radical distribution investigation in irradiated solid substances: influence of let and spur effects. *Radiat Eff* 3(1):61–64. doi:10.1080/00337577008235617
 78. Raitsimring AM, Tsvetkov YD, Moralev VM (1973) LET-effects on free-radical yields and spatial-distribution in irradiated methanol—investigation by means of ESR and ESE methods. *Int J Radiat Phys Chem* 5(3):249–269

79. Shelimov BN, Fok NB, Voevodsky VV (1963) The photochemical decomposition of alcohols at low temperatures: the kinetics of the decomposition of methyl alcohol. *Kinet Katal* 4(4):539–548
80. Gray LH (1952) The energy transfer from ionizing particles to an aqueous medium and its bearing on the interpretation of radiochemical and radiobiological change. *J Cell Physiol Suppl* 39(Suppl 1):57–74
81. Fröhlich H, Platzman RL (1953) Energy loss of moving electrons to dipolar relaxation. *Phys Rev* 92(5):1152–1154. doi:10.1103/PhysRev.92.1152
82. Magee JL, Burton M (1951) Elementary processes in radiation chemistry. II. Negative ion formation by electron capture in neutral molecules 1,2,3. *J Am Chem Soc* 73(2):523–532. doi:10.1021/ja01146a006
83. Zimbrick J, Kevan L (1967) Evidence for trapped dielectrons in ice. *J Am Chem Soc* 89(10):2483–2484. doi:10.1021/Ja00986a043
84. Kevan L, Renneke DR, Friauf RJ (1968) Optical absorption spectrum of trapped dielectrons in alkaline ice. *Solid State Commun* 6(7):469–471 doi:10.1016/0038-1098(68)90057-4
85. Raitsimring AM, Samoilova RI, Moralev VM, Tsvetkov YD (1976) Spatial distribution of trapped electrons and O⁻ in b- and g-irradiated NaOH glasses at 77 K. In: Hedvig P, Schiller R (eds) *Proceedings of the fourth Tihany symposium on radiation chemistry*. Akadémiai Kiadó, Budapest, pp 691–700
86. Raitsimring AM, Moralev VM, Tsvetkov YD (1975) Electron-spin echo study of detailed track structure in irradiated frozen aqueous-solutions of sulfuric and phosphoric acids. *High Energy Chem* 9(6):449–454
87. Samoilova RI, Raitsimring AM, Tsvetkov YD (1980) The structure of radical tracks in methanol irradiated by tritium beta-particles. *Radiat Phys Chem* 15(4):553–559. doi:10.1016/0146-5724(80)90070-9
88. Brustolon M, Zoleo A, Lund A (1999) Spin concentration in a possible ESR dosimeter: an electron spin echo study on X-irradiated ammonium tartrate. *J Magn Reson* 137(2):389–396. doi:10.1006/jmre.1998.1671
89. Ichikawa T, Yoshida H (1984) Spatial-distribution of paramagnetic entities in gamma-irradiated 2-methyltetrahydrofuran glass as studies by the electron-spin echo method. *J Phys Chem* 88(15):3199–3203. doi:10.1021/J150659a013
90. Ichikawa T, Wakasugi S, Yoshida H (1985) Structure of spurs in gamma-irradiated alcohol matrices determined by electron spin-echo method. *J Phys Chem* 89(16):3583–3586. doi:10.1021/J100262a032
91. Ichikawa T, Kawahara S, Yoshida H (1985) Local-distribution of alkyl radicals in gamma-irradiated polyethylene studied by electron-spin echo method. *Radiat Phys Chem* 26(6):731–737. doi:10.1016/0146-5724(85)90115-3
92. Dzuba SA, Raitsimring AM, Tsvetkov YD (1979) Distance distribution of radical-paramagnetic ion-pairs studied by the electron-spin echo method-spatial regularities of radical diffusion in glassy alcohols. *Chem Phys* 44(3):357–365. doi:10.1016/0301-0104(79)85219-2
93. Kononov VV, Dzyuba SA, Raitsimring AM, Salikhov KM, Tsvetkov YD (1980) Spatial-distribution of hydrogen in ion-atom pairs formed by the photolysis of frozen acidic solutions of chromium and iron ions. *High Energy Chem* 14(6):406–411
94. Dzyuba SA, Raitsimring AM, Tsvetkov YD (1981) Range distribution of cation-electron pairs formed in the gamma-radiolysis of a vitrified solution of sulfuric-acid. *High Energy Chem* 15(1):30–34
95. Borbat P, Freed JH (1999) Multiple-quantum ESR and distance measurements. *Chem Phys Lett* 313:145–154
96. Maryasov AG, Tsvetkov YD, Raap J (1998) Weakly coupled radical pairs in solids: ELDOR in ESE structure studies. *Appl Magn Reson* 14(1):101–113
97. Jeschke G, Polyhach Y (2007) Distance measurements on spin-labelled biomacromolecules by pulsed electron paramagnetic resonance. *Phys Chem Chem Phys* 9(16):1895–1910. doi:10.1039/B614920k

98. Jeschke G (2012) DEER distance measurements on proteins. *Annu Rev Phys Chem* 63(1):419–446. doi:10.1146/annurev-physchem-032511-143716
99. Pannier M, Veit S, Godt A, Jeschke G, Spiess HW (2000) Dead-time free measurement of dipole-dipole interactions between electron spins. *J Magn Reson* 142(2):331–340
100. Raitsimring A, Peisach J, Lee HC, Chen X (1992) Measurement of distance distribution between spin labels in spin-labeled hemoglobin using an electron-spin echo method. *J Phys Chem* 96(8):3526–3531
101. Bode BE, Margraf D, Plackmeyer J, Durner G, Prisner TF, Schiemann O (2007) Counting the monomers in nanometer-sized oligomers by pulsed electron-electron double resonance. *J Am Chem Soc* 129(21):6736–6745. doi:10.1021/Ja065787t
102. Milov AD, Ponomarev AB, Tsvetkov YD (1984) Modulation beats of signal of double electron-electron resonance in spin-echo for biradical systems. *Zhurnal Strukturnoi Khimii* 25(5):710–713
103. Bowman MK, Maryasov AG, Kim N, DeRose VJ (2004) Visualization of distance distribution from pulsed double electron-electron resonance data. *Appl Magn Reson* 26(1–2):23–39
104. Saxena S, Freed JH (1997) Theory of double quantum two-dimensional electron spin resonance with application to distance measurements. *J Chem Phys* 107(5):1317–1340
105. Borbat PP, Mchaourab HS, Freed JH (2002) Protein structure determination using long-distance constraints from double-quantum coherence ESR: study of T4 lysozyme. *J Am Chem Soc* 124(19):5304–5314. doi:10.1021/Ja020040y
106. Milov AD, Salikhov KM, Shirov MD (1981) Application of ELDOR in electron-spin echo for paramagnetic center spatial distribution in solids. *Fiz Tverd Tela* 23(4):975–982
107. Pusep AY, Shokhirev NV (1984) Application of a singular expansion in the analysis of spectroscopic inverse problems. *Opt Spektrosk* 57(5):792–798
108. Bowman MK, Becker D, Sevilla MD, Zimbrick JD (2005) Track structure in DNA irradiated with heavy ions. *Radiat Res* 163(4):447–454. doi:10.1667/rr3338
109. Marrale M, Brai M, Barbon A, Brustolon M (2009) Analysis of the spatial distribution of free radicals in ammonium tartrate by pulse EPR techniques. *Radiat Res* 171(3):349–359. doi:10.1667/Rr1358.1